
.

Fundamentals of

EXOPLANETS and ASTROBIOLOGY

**From the origin of the universe, stars and elements,
and the creation of solar systems and exoplanets,
to the arise and development of life**

Uffe Gråe Jørgensen, February 2023.

**Part 2: Stellar evolution, supernovae, red giants, and formation of the
elements in stars**

for the lectures February 14, 16 and 21, 2023.

For astrobiology students, Univ.Cph.2023

1

Nucleosynthesis in stars

The first modern suggestion for how the Sun gets its energy to shine is due to Lord Kelvin slightly before the turn of the 20th century. He envisioned that the energy comes from gravitational contraction and corresponding conversion of potential energy. The virial theorem tells us that half of the potential energy will be converted into kinetic energy, and the other half will be transformed into radiation. By calculating the total potential energy release from a gas of one solar mass, $M_{\odot} = 1.99 \cdot 10^{30}$ kg, contracting from infinite to the present solar radius, $R_{\odot} = 6.96 \cdot 10^8$ m, it is therefore possible to compute how much energy can be radiated away due to the contraction. By dividing this number with the solar luminosity, $L_{\odot} = 3.83 \cdot 10^{26}$ W, one gets (under the assumption that the solar luminosity has been more or less constant throughout its life), the present age of the Sun. We will get a number of approximately 20 million years from the above exercise. It was not known when Kelvin developed his theory, that even the Earth is much older than 20 million years, and maybe even more important, that this age is far smaller than the (now very well established) value of 4.57 billion years one can determine for the age of the meteorites from measuring the relative abundances of radioactive elements. Even though there is no direct way of determining the age of the Sun, it is believed that the Sun and the solar system (including the Earth and the meteorites) were formed at the same time, and that the meteoritic age therefore also is the age of the Sun. So, in conclusion, the gravitational energy is not sufficient for the stars to shine like the Sun for long enough time-scales. The potential energy from the contraction is, however, an important energy source during the initial contraction phase where the proto-solar disk is formed.

The only energy source we know of that can give the amount of energy necessary to let the Sun shine with approximately its present luminosity for the meteoritic time-scale, is conversion of matter to energy from $E = mc^2$, and the most powerful conversion we realistically can envision is the fusion of hydrogen to helium, as first suggested by H.Bethe, v.Weizsäcker and others in the end of the 1930s. The relative mass difference between 4 hydrogen atoms and 1 helium atom is

$$\frac{4m_H - m_{He}}{4m_H} = \frac{0.0287}{4.0313} = 7.12 \cdot 10^{-3} \quad (1.1)$$

In other words, 0.7% of the hydrogen mass is converted into energy when hydrogen fussionates to become helium.

The energy release from one kg of hydrogen is therefore $E[J] = 1[\text{kg}] \cdot 0.00712 (\text{c}[\text{m/s}])^2 = 6.4 \cdot 10^{14}$ J, and the mass lost would be 7 gram. In other words, by accepting this process as the source for the solar energy, we postulate that the Sun looses mass with a rate of $7[\text{g}]L_{\odot}/E = 4.19 \cdot 10^{12}$ g per second (= 4 million tons/s!). If it has been shining with the same luminosity during all the 4.57 billion years it will have converted $8.6 \cdot 10^{28}$ kg of hydrogen into helium and hereby lost a mass of $6 \cdot 10^{26}$ kg (= $100 M_{\oplus}$). Although these numbers undoubtedly sounds overwhelming, they correspond to that only $8.6 \cdot 10^{28}/X M_{\odot} = 6\%$ of the total amount of

hydrogen in the Sun has been burnt to helium during the last 4.57 billion years, and that only $6 \cdot 10^{26} / M_{\odot} = 0.03\%$ of the total solar mass has been lost by conversion into energy. Here X denotes the fraction of the solar mass, M_{\odot} , which is hydrogen, and L_{\odot} is the solar luminosity $L_{\odot} = 3.9 \cdot 10^{26}$ Watt.

The hydrogen to helium fusion process is therefore realistic in terms of being able to account for the solar radiation and stability. The Sun would be able to shine with the present luminosity for

$$t_{\odot} = E M_{\odot} / L_{\odot} = 6.4 \cdot 10^{14} \cdot 1.99 \cdot 10^{30} / 3.9 \cdot 10^{26} = 3.26 \cdot 10^{18} \text{ sec} = 1.03 \cdot 10^{11} \text{ years}, \quad (1.2)$$

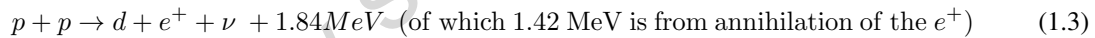
so (as opposed to the available potential energy) there is plenty of energy available in the process of converting hydrogen to helium.

In practice the solar luminosity will increase to $\approx 10^4 L_{\odot}$ by the end of the solar evolution (about 7.5 billion years from now), the hydrogen will not burn only to helium, but further to carbon and oxygen, and around half of the present solar mass will be lost via a wind during the final stages of the solar evolution (of which some of the material has been nuclear processed and some not). Therefore we do not expect a solar lifetime of 10^{11} years, but rather $1.2 \cdot 10^{10}$ years, but this is irrelevant for the present discussion. The important conclusion here is that if nuclear processes can run in the interior of stars, they can plentifully deliver the energy to make the stars shine as we see them today, over very long time-scales. If further the processed material can come out of the stars after nuclear processing (which is not trivial, and which will be the subject of the following chapters), then the nuclear reactions in the interior of stars can be a realistic explanation of the existence in nature of elements other than hydrogen and helium, including those that form our surroundings on Earth, and life itself.

1.1 The *pp*-chains and the solar neutrino problem

When the first nucleosynthesis took place in stars, the Big Bang free neutrons had of course long decayed away (or been included in helium), and the deuterium formation mechanism from Big Bang can therefore not be repeated in stars. This is the basic reason why the nuclear time-scale is billions of years in stars while it was minutes in the Big Bang. Two processes have been suggested as the first nucleosynthesis in stars – the *pp* process and the *CNO* bi-cycle.

The *pp* chain(s) start with



This process requires much longer times than the very short time-scale of the Big Bang nucleosynthesis. The process is quite unusual compared to most other nuclear processes. For the reaction to take place, the protons have to β^+ decay during the time of their closest approach. Since this decay is governed by the weak interaction, it is very unlikely. Basically this is the reason why the Sun doesn't explode, but can keep shining for biological time-scales. If the first possible nuclear reaction involving hydrogen was as quick as the following reactions, then the Sun would burn its fuel as an explosion. On the other hand the slowness of reaction Eq.1.3 is also the reason that the deuterium abundance is never increased any place in nature (other than in the Big Bang), but only constant or decreasing with time. Deuterium is immediately destroyed under any equilibrium conditions where it can be produced, and the primordial deuterium is readily burned already during the stellar contraction phase before the stars settle on the main sequence, and it delivers nuclear fuel even to substellar objects as small as $15 M_{\text{Jupiter}}$ or smaller.

The next reaction in the *pp* chain is



but after this the *pp* process branches into 3 chains (see Fig. 1.1.). *pp* – 1 proceeds with the reaction ${}^3\text{He}({}^3\text{He}, 2p){}^4\text{He}$ and takes place in 86% of the time (in the Sun), while *pp* – 2 and *pp* – 3 both proceed with ${}^3\text{He}(\alpha, \gamma){}^7\text{Be}$, where-after they diverge into the two sub-branches shown in the table below, which takes place 14% and 0.02% of the time, respectively.

In the early 1960s Raymond Davis sat up an experiment to test our understanding of the solar energy production, by measuring the number of neutrinos coming from the Sun. While the energy carried by the

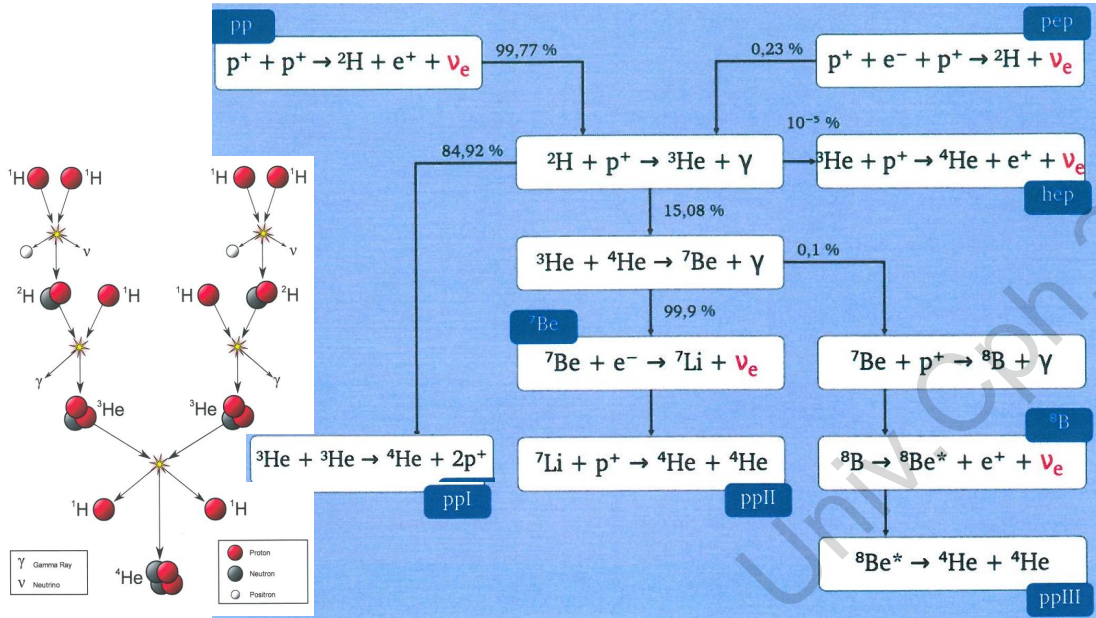


Figure 1.1. The relative contribution of the pp-1, pp-2, and pp-3 reaction chains. Inset illustrates the pp-1 process in graphical detail.

photons from the solar interior takes millions of years to reach the surface (because of many absorptions and re-emissions on the way from the interior to the surface), the neutrinos are basically not absorbed during their passage from the interior to the surface, and therefore reach us only 8 minutes (the light-distance from the Sun to the Earth) after the nuclear reaction which produced them. It was considered a serious problem for our understanding of the energy production in stars, when Davis' measurements showed less than 1/3 of the predicted neutrinos. However, it must be remarked that Davis' experiment mainly is sensitive to the $pp - 3$ neutrinos and that the $pp - 3$ branch is responsible for only 0.02% of the solar energy production. It was therefore crucial to set up other experiments to test other parts of the neutrino energy spectrum. The results of these experiments are summarised in Tab. 1.1.

While Davis' experiment is based on the reaction



the later Kamiokande II experiment in Japan relies on the reaction with water. It is still only the $pp - 3$ neutrinos which are observable, but the experiment is sensitive to another (higher) energy part of the neutrinos energy spectrum. The result of the Kamiokande experiment was in better agreement with the theoretical predictions than was the chlorine experiment, with a ratio of observed to predicted neutrino flux of less than 2. Finally, in 1990 the international *Gallex* experiment set up in the Mount Blanc tunnel between France and Italy, resulted in the first measurements of the neutrinos from the main branch (Eq. 1.3 and top line of Fig. 1.1) of the pp chain. It was predicted that 20 atoms per month of the 30 tons of the metal gallium the detector consists of, would react with a neutrino, giving rise to the reaction



and the results came out with only 30% less neutrinos than predicted (or 9% if one stretches the numbers in Tab. 1.1 within 1σ). This discrepancy would most likely not have been considered alarming had it been the first measurement of the three, and a likely reason for the discrepancy is rooted in the neutrino physics;

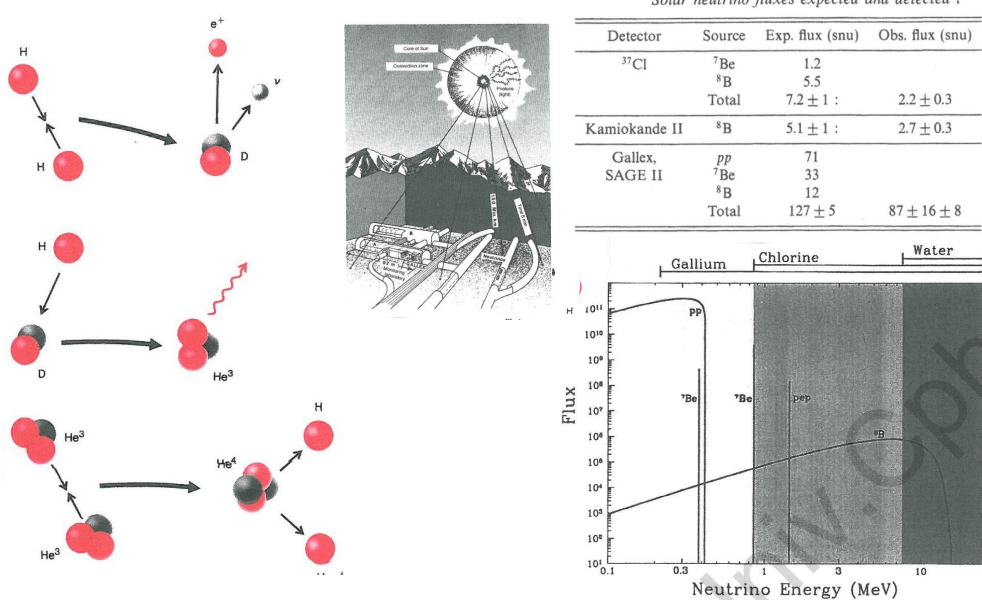


Table 1.1. Measured and predicted neutrino fluxes for various experimental setups. The unit SNU (solar neutrino unit) is 10^{-36} events per target atom per second.

for example a small mass of the neutrinos would enable them to oscillate between ν_e and ν_μ on their way from the Sun, which would affect the expected number of events. In conclusion, it is consistent with lifetime, luminosity, and energy requirements, and with neutrino experiments, to postulate that the Sun gets its energy by converting hydrogen to helium (via the *pp*-process). It is therefore fair to postulate that the motor of life is the heat from an enormous nuclear fusion reactor, and that the first step after the Big Bang in building the material living organisms is made of, is the nuclear waste of this same reactor.

1.2 The CNO bi-cycle; hydrogen to helium burning in hot environments

If smaller amounts of carbon, nitrogen, and oxygen (CNO) already exist in the stellar gas (from earlier generations of stars), these nuclei can act as catalysts for an alternative route of producing a helium atom from 4 hydrogen atoms. The process is actually two separate cycles (and is therefore often called the CNO *bi*-cycle), the CN cycle and the ON cycle (see Fig. 1.2). The branching between the two depends on detailed conditions in the stars.

As a whole, the energy production in the CNO bi-cycle is proportional to T^{18} (temperature to the power 18), while the *pp*-chain depends on T^4 . The ratio of the energy production from the two processes is therefore proportional to T^{14} , with the CNO bi-cycle dominating the energy production at higher temperatures. For the Sun where the central temperature is 15 million degrees, only 1% of the energy comes from the CNO bi-cycle, but already at 16 million degrees the two processes will contribute equal amounts of energy.

Although the CNO nuclei act as catalysts only, the differences in reaction rates between the different parts of the cycles cause a steady-state ratio between all the isotopes to be established. This ratio will freeze into the CNO ratios when the reaction is terminated (e.g., when there is no more hydrogen), and these ratios will eventually manifest themselves when the CNO processed material is exposed to the visible surface later in the stellar evolution. The measurement of the CNO isotopic ratios in spectra of stars in the late stages of

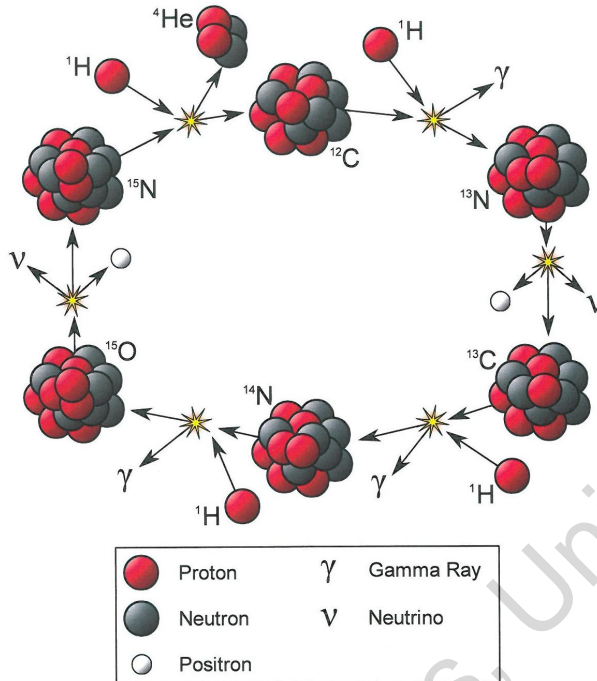


Figure 1.2. The CNO bi-cycle.

evolution therefore holds important information about the conditions for nuclear processes that have prevailed earlier in the star's evolution. Since the reaction $^{14}\text{N} + \text{p} \rightarrow ^{15}\text{O}$ is the slowest reaction in the CNO bi-cycle (see Fig. 1.2), the steady-state will result in a (strong) overabundance of ^{14}N relative to carbon and to the other isotopes of nitrogen. Since the reaction $^{15}\text{N} + ^1\text{H}$ has approximately 10^4 times higher likelihood of resulting in $^{12}\text{C} + ^4\text{He}$ (i.e., the CN cycle) than in $^{16}\text{O} + \gamma$ (the ON cycle), the main effect of the ON cycle is to effectively consume the amount of ^{16}O that was originally present in the gas, and convert it into ^{14}N . Similarly, the steady state ratio of $^{12}\text{C}/^{13}\text{C}$ is reduced from the solar value of 89 to 3.5 in the steady-state CNO burning; a signature often seen in the spectra of late type stars.

1.3 The conversion of helium to carbon and oxygen

The non-existence of stable nuclei with mass number 5 and 8 was the major reason that the Big Bang nucleosynthesis stopped at the production of hydrogen and helium. Numerical calculations have shown that in the stars the nuclei-5-and-8-problem will be overcome by the long time-scales involved, in the sense that stars can afford that only a very tiny fraction of the reactions successfully leads to a new stable nucleus. A temperature sensitive equilibrium exist between 2α and the highly unstable ^8Be which has a half-life for decay back into 2α of 10^{-15} seconds. If density and temperature is high enough, a reaction may some times take place between the unstable ^8Be and another α before the decay, giving rise to a ^{12}C nucleus. However, the produced ^{12}C nucleus is in an excited state 7.65 MeV above its ground state, and in most cases the compound

	^{12}C	^{13}C	^{14}N	^{15}N	^{16}O	^{17}O
CNO eql at $3 \cdot 10^7 \text{ K}$	1.6	0.39	97	3×10^{-3}	1.3	4.3×10^{-4}
Solar abundances	28	0.30	8.3	3×10^{-2}	64	8.3×10^{-3}

Table 1.2. The CNO steady-state equilibrium values at $3 \cdot 10^7 \text{ K}$ compared to the solar abundances.

nucleus will decay back into 3α . It, however, also have a tiny probability of electro-magnetic decay into the ground state, in which case a successful



reaction has taken place. We call the reaction in Eq. 1.7 for *the triple-alpha* reaction. The balance is illustrated in Fig. 1.3.

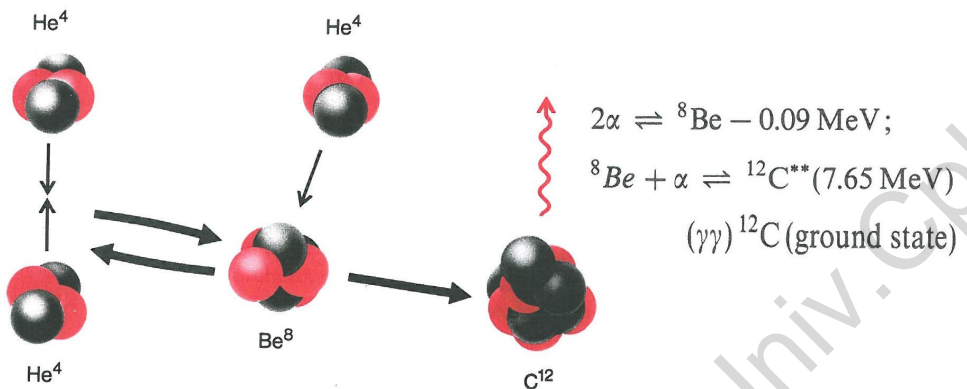


Figure 1.3. Details of the triple α reaction, converting three 4He to one ${}^{12}C$

Once the ${}^{12}C$ atom has been created, successive reactions adding α particles will create the most abundant nucleus in the mass range between carbon and iron. Of particular importance is the reaction



The cross section for this reaction was long thought to be relatively small, but later laboratory experiments have shown its value to be large enough that virtually all carbon in the core of low- and intermediate-mass stars is converted from carbon to oxygen. Since the stellar remnant from the bulk of stars is a white dwarf created in the central region during the late stages of evolution, the most common type of white dwarfs are now believed to consist mainly of oxygen rather than carbon (so, unfortunately the most common end-product of stars, can no longer be claimed to be eternal diamond-like objects spread throughout our galaxy!).

As we will see later, the carbon/oxygen in the white dwarfs will, however, never be recycled to interstellar space, and therefore the process Eq. 1.8 in the center of low and intermediate mass stars will have only little effect on the cosmic nucleosynthesis. During the final stellar evolution where a white dwarf is created in the center, a shell of material around the core exist where helium is converted to carbon from the above reaction (Eq. 1.7). Here the physical conditions are quite different from the conditions in the center, and the reaction Eq. 1.8 will not take place and helium will only be converted to carbon. Since, as we will see in a following chapter, most of the carbon in nature, and hence the carbon biological material is based upon, most likely comes from this helium shell burning process in intermediate mass stars, the reaction rate Eq. 1.8 has strong direct implication for our existence.

1.4 The creation of the elements between oxygen and iron.

The creation of the elements heavier than carbon and oxygen is much more complex than the creation of the elements up to and including carbon. The reason is that many reactions can lead to the various nuclei, and one has to take all these channels into account simultaneously. In addition, the nuclei can also be destroyed again, in particular at high temperatures. The results are therefore not easily described analytically, but one often has to rely on the results of the numerical scheme.

A glance at Fig. 1.4, however, show that nuclei with atomic mass number a multiplum of 4 are considerably more abundant than the elements next to them. Most pronounced and abundant are the nuclei ${}^{12}C$, ${}^{16}O$,

^{20}Ne , ^{24}Mg , ^{28}Si , ^{32}S , ^{36}Ar , ^{40}Ca , and ^{56}Fe . These nuclei are obviously formed by reactions whose net results are successive captures of an α particle. Approximately 98% of the mass in the universe is hydrogen and helium ($\sim 1\alpha$), while approximately 3/4 of the rest is made up by carbon ($\sim 3\alpha$) and oxygen ($\sim 4\alpha$).

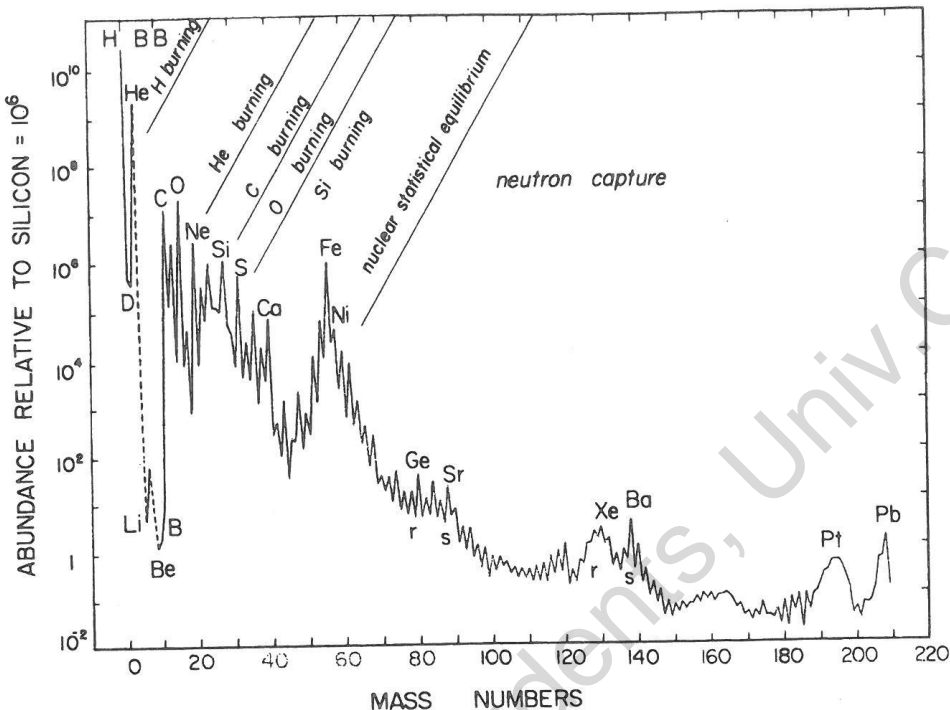


Figure 1.4. The “cosmic” (\equiv solar) abundance of the elements, per 10^6 silicon atoms, as function of their atomic mass numbers. Some elements and major production processes are indicated in the figure, too.

In addition to the “ α -tops”, we note from Fig. 1.4 also the pronounced “under-abundance” of the primordial nuclei between helium and carbon, which can be understood from the Big Bang nucleosynthesis and Eq. 1.7. Remark also the relative under-abundance of nuclei in the region between Ca and Fe, and the relative over-abundance of the iron-group elements (i.e. elements around Cr, Fe, Co, and Ni), relative to the general trend (i.e., relative to a “smoothly declining average curve”). Qualitatively the over-abundance around the iron-group can be understood from Fig. 1.5, as an effect of the strong binding energy of the nuclei with mass number close to iron, which is also the basic explanation for the corresponding under-abundance of elements between Ca and Fe.

The first reaction on the build up of carbon takes place already simultaneously with the triple alpha burning process, to form oxygen (Eq. 1.8). It is believed that most of the carbon is burned to oxygen in the helium burning central region in normal stars. Even some oxygen burning to neon can take place in the triple alpha burning region, while further burning is rare in the 3α zone.

After the formation of carbon and oxygen and the exhaustion of helium, carbon will react with itself at temperatures typically around 500 million K and above. The most abundant reactions being:



The produced protons and alpha particles will find them selves at temperatures far higher than during the previous hydrogen and helium burning cycles, and they will immediately react with everything around. The net outcome of this chain of reactions is that each pair of ^{12}C – ^{12}C will have released about 13 Mev, and been transformed into mainly ^{16}O , ^{20}Ne , ^{24}Mg , and ^{28}Si .

At temperatures of approximately 1 billion K, also the oxygen can react with itself, mainly through the channels



Again the protons and alpha particles will quickly react and give rise to many different nuclei, but the end-product will be a release of ≈ 16 MeV per oxygen pair, and creation mainly of ${}^{28}\text{Si}$.

At even higher temperatures the photon energies are so high that many nuclei are photo-disintegrated, and an equilibrium between the nuclei formation from nuclear reactions and photo-disintegration is established. If n_{ij} represent the number density of a given nucleus, Q the energy required to disintegrate this nucleus, and n_i and n_j the number density of its disintegrated parts, then this equilibrium can be expressed as

$$\frac{n_i n_j}{n_{ij}} \approx T^{2/3} e^{-Q/kT} \quad (1.11)$$

At around 3 billion K, ${}^{28}\text{Si}$ is disintegrated by energetic photons creating a "soup" of protons and alpha particles together with Al, Mg, Ne, and other nuclei. These nuclei will themselves photo-disintegrate, and a huge number of different reactions will take place simultaneously, involving both disintegration and build up of the original and other nuclei, including heavier nuclei with stronger binding energies. Due to the larger binding energy of these heavier nuclei, they will have a tendency to better resist the photo-disintegration, and the balance between the lighter and the heavier nuclei will therefore gradually shift toward the tightly bound iron-group elements.

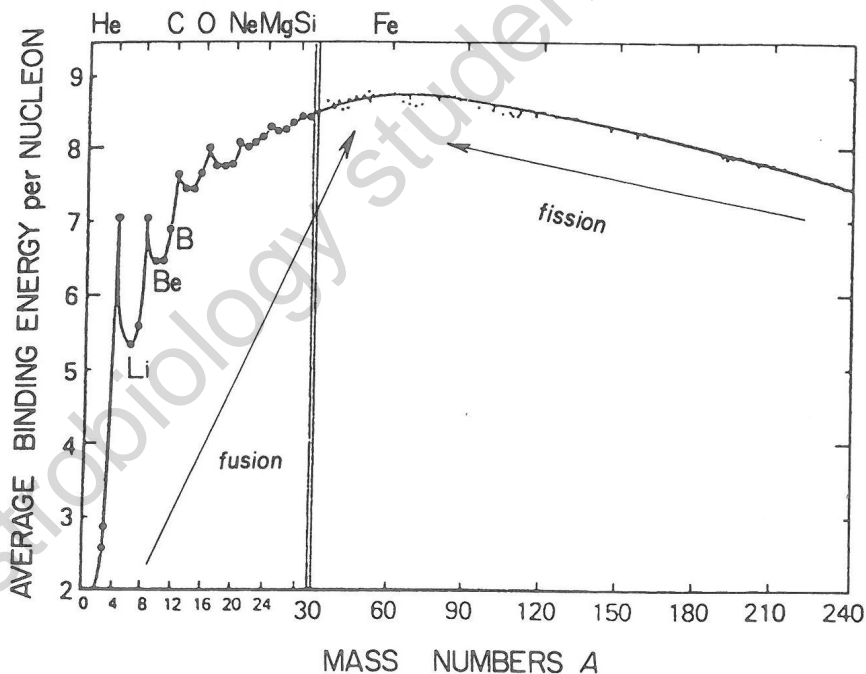


Figure 1.5. The average binding energy per nucleon as function of atomic mass number. The binding energy has a maximum for the ${}^{56}\text{Fe}$ nucleus, and energy can therefore be gained by fusion ("combination") of elements lighter than iron, or by fission ("breaking up") of elements heavier than iron.

We can therefore qualitatively understand that we will end up with an excess of iron-group elements, and a corresponding deficiency of the elements right below (in mass number) the iron-group, as we see it in

Fig. 1.4. The duration of this last epoch, which we could call the "Si-melt-down", is not very long, since the burning rate (i.e., the stellar luminosity) is high and the net energy that can be gained, even from transforming Si to Fe, is quite small (as is seen from Fig. 1.5). For a 25 solar mass star, for example, it takes close to 8 million years to build up the silicon mass from burning the hydrogen, but it takes only ≈ 1 day to transform all the produced Si to iron (see Tab. 1.3).

1.5 Elements heavier than iron: the *r*- and *s*-process elements.

It is seen from Fig. 1.5 that one cannot gain energy from fusion of nuclei to anything heavier than iron. On the contrary, as is well known from a conventional nuclear power plant, one can gain energy by fissioning heavy nuclei down toward the iron regime. All of this is because of the maximum in nuclear binding energy around the iron-group elements, but then how are the elements heavier than iron created in nature?

Obviously the process requires energy, and we must therefore look for places where energies are available in abundance. Second, neutrons are the particles which most easily penetrate the Coulomb barrier into the nucleus, so we will further look for places where possible free neutrons are available. In principle one could envision all kind of processes and environments that could lead to the formation of the stable, heavy nuclei, but in practice nature, fortunately, seems to have simplified the picture for us, such that all the heavy isotopes can be explained by two extreme processes: One process where the flux of neutrons have been so high that the produced nuclei are all the time hit by a new neutron before they can find time to decay back to the line of stable nuclei in the neutron versus protons diagram (the so-called " β -stability valley"), and another process where the neutron flux was so modest that a produced nucleus was never hit by a second neutron before it β decayed. With very few exceptions, there are no nuclei which seem to have been produced by a neutron flux in-between these two extremes (i.e., where the probability for a capture and for a decay were of the same order). We call the first process for *rapid neutron capture* or the *r*-process, and the latter for *slow neutron capture* or the *s*-process.

Fig. 1.6 shows the position of all the stable heavier nuclei in nature as function of proton- and neutron-number. The sum of all these heavy elements makes up for quite a small fraction of the mass in the universe. However, there is a larger number of different stable isotopes with atomic number higher than iron than there are stable isotopes lighter than iron, and we can therefore expect a large amount of information about the nucleosynthesis to be hidden in the heavy elements.

It is seen in Fig. 1.6 that all the stable nuclei fall along a narrow band in the diagram, called the β -stability valley and representing nuclei with a slight overabundance of neutrons compared to protons. Nuclei with an over-abundance of neutrons will β^- -decay toward the β -stability valley. In principle nuclei with an over-abundance of protons could β^+ -decay toward the β -stability valley as well.

In Fig. 1.6 the number of protons in the nuclei are plotted against the number of neutrons, and all (heavy) stable isotopes are marked by a dot in the diagram. It is seen that in general all heavy elements (i.e., nuclei with a given proton number) have several stable isotopes (i.e. possible neutron numbers). The stable isotope ^{56}Fe is marked specifically. Since we know from Fig. 1.4 that iron is the most abundant of the elements after silicon, and from Fig. 1.5 that it is the last to be produced exo-thermal (i.e., by gain of energy), it is common to start reaction networks for calculating the abundances of the (endo-thermically produced) elements (isotopes) heavier than iron, by adding neutrons to ^{56}Fe . If this is done by always letting a produced unstable isotope decay back onto the β stability line before a new neutron is added, the produced nuclei will move from the position of ^{56}Fe and up through the diagram along the so-called *s*-process path, which is shown as a solid line in the diagram (if we didn't start with ^{56}Fe , but with another abundant element/isotope, we would usually just start our calculation somewhere else along this *s*-process path). It is seen that most of the stable nuclei lies along the *s*-process path. This means that they can be formed via the *s*-process channel, but not necessarily that they can only be formed this way. For some of the isotopes along the *s*-process path therefore only a certain percent are formed via the *s*-process path, while for some 100% of the nuclei are *s*-process. Summing all the percentages, ends with predicting that approximately 2/3 of the nuclei heavier than iron are *s*-process produced isotopes. The dots to the right and to the left of the *s*-process path are unreachable by the *s*-process (on ^{56}Fe), and are either pure *p*-process nuclei (i.e., with excess protons), or pure *r*-process nuclei. There are no generally accepted standard theory for the origin of the *p*-process elements.

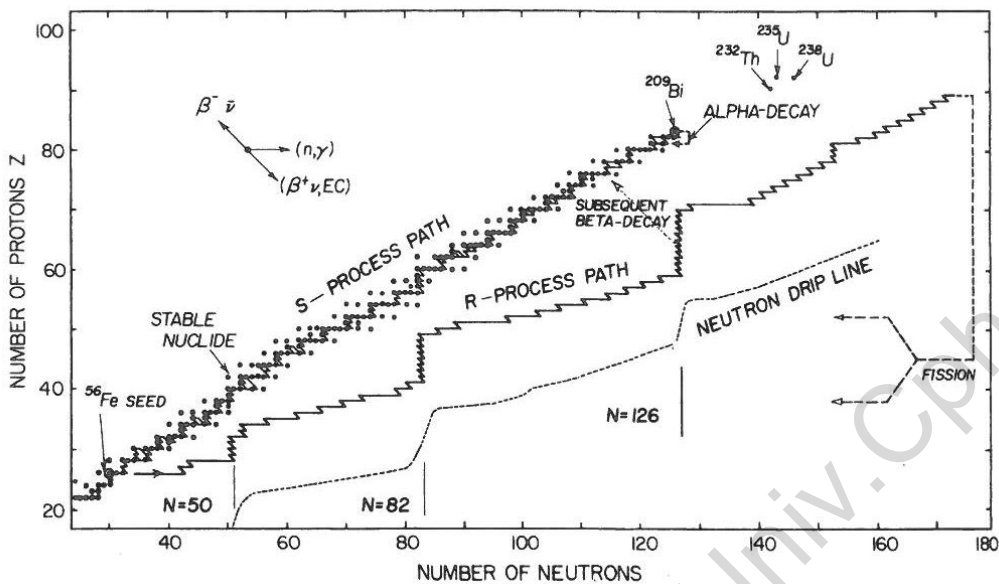
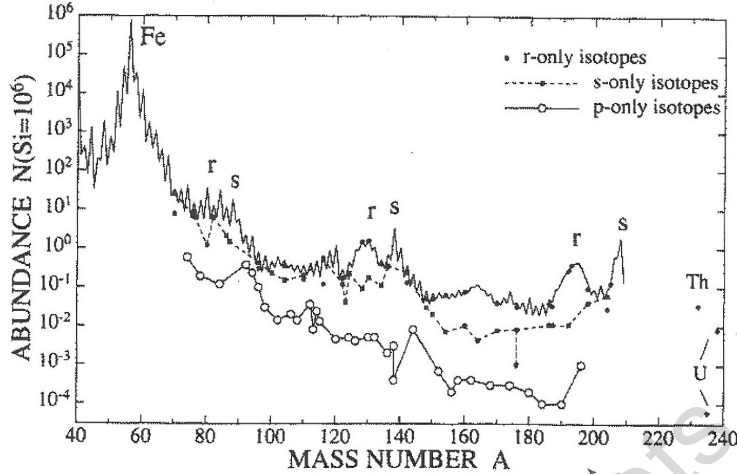


Figure 1.6. The β stability valley in a diagram showing the number of protons versus number of neutrons. Dots represent the stable isotopes in nature. Line marked *s*-process path represent the movement a nucleus will follow when exposed to the slow neutron capture process. *r*-process path indicates the movement a ^{56}Fe nucleus will move if exposed to a density of 10^{24} neutrons per cm^3 at a temperature of 10^9 K . Arrows in upper left corner show direction of nuclear movement in the diagram from β decay and from neutron capture.

In Fig. 1.6 are also shown the path along which an ^{56}Fe nucleus would move if exposed to the *r*-process in a gas of $T=10^9\text{ K}$ with a neutron density of 10^{24} neutrons per cm^3 (marked as “*r*-process path”). The longer time the nucleus is exposed to this neutron flux and temperature, the further up the line it will move. At very high neutron numbers the nuclei would fissionate before they could manage to β -decay, as is illustrated in the upper right of the figure. The *neutron drip line* in Fig. 1.6 shows the maximum number of neutrons it is possible to add to a given element. Both the *r*-process path and the neutron drip line show the effect of the closed shell nuclear structure at $N=50$, 82 , and 126 (corresponding to the closed shell electronic structure in atoms).

It is due to decades of experimental effort to collect β -decay half-lives, neutron capture cross sections, and other relevant information for almost all of the nuclei in the region around the β -stability valley, that it has been possible to make figures as Fig. 1.6. Such extensive data are collected in the so-called chart of the nuclides. Numerical simulations based on data in the chart of nuclides show that very strong neutron exposures during approximately 1 second will create a relative abundance of the *r*-process nuclei as the one we see in the Sun. The only place we know of where sufficiently high temperatures and neutron densities exist, is in supernova explosions. Since furthermore the collapse phase and the corresponding neutrino and neutron formation epoch in the supernova explosion last of the order 1 second, we identify this phase with the *r*-process formation place. Remark that according to these (realistic) ideas, all the *r*-process elements in nature have to be created in an ongoing process which takes place over a total time of about 4 seconds per century in a typical galaxy like our own (i.e., a second in each of the 4 supernovae per century that are typical for normal galaxies; see later). The process during these few seconds obviously have to be extremely efficient and powerful. About 1/3 of the isotopes heavier than iron which we find in nature are *r*-process isotopes.

When the neutron radiation stops after an *r*-process neutron burst, all the nuclei formed along the *r*-process path shown in the Fig. 1.6, will rapidly decay down to the bottom of the β -stability valley. The decay route down to the line of stable nuclei will not be the same when the nuclei decays from the *r*-process position



Element	$\log N$	s-weak	s-main	r
37 Rb	2.40	.14	.39	.47 ± .10
38 Sr	2.93	.09	.77	.14 ± .07
39 Y	2.22	.04	.85	.11 ± .06
40 Zr	2.61	.02	.78	.20 ± .03
56 Ba	2.21	.01	.88	.11 ± .02
57 La	1.20	.01	.75	.25 ± .08
58 Ce	1.61	.01	.77	.23 ± .01
59 Pr	0.71	.01	.45	.54 ± .09
60 Nd	1.47	.00	.46	.53 ± .03
62 Sm	0.97	.00	.30	.70 ± .03
63 Eu	0.54	.00	.03	.97 ± .06
66 Dy	1.15	.00	.12	.88 ± .15

The distribution between p-, s- and r-process abundances (upper left), examples of relative s- and r-contribution to specific isotopes (lower left), and the principle of shielding from beta-decay in the formation of pure s-, pure r-, and mixed abundance isotopes.

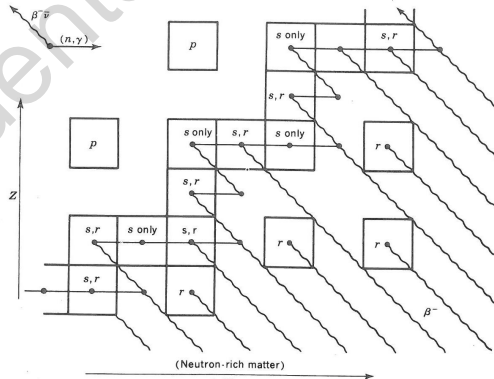


Figure 1.7. The abundance of the heavy elements. The full drawn line in the upper panel is the same as in Fig. 1.4, but on this figure is also shown the separate contribution of isotopes from the *s*-process, the *r*-process, and the *p*-process. Remark that the illustrated abundance for a heavy element of a given mass number, generally is the sum of the abundances of several isotopes and elements. Regions of the diagram dominated by either *r*-process or *s*-process isotopes are marked with an *r* or and *s* in the figure. The table (lower left) gives specific examples of the relative abundance distribution between *s*-process and *r*-process for some specific isotopes, while the lower right panel illustrates the general principle of shielding.

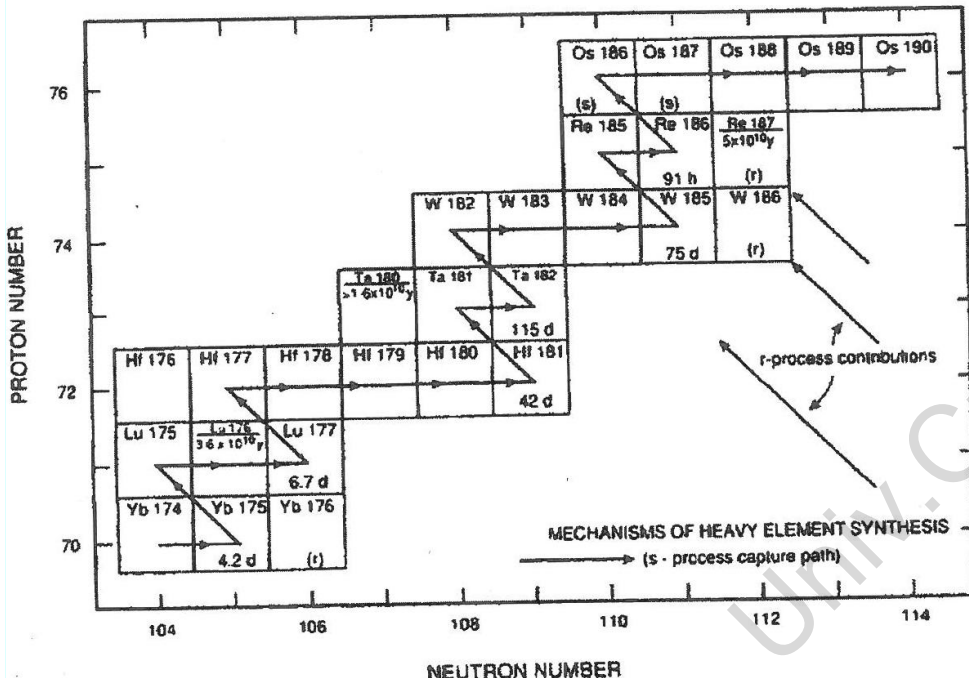


Figure 1.8. Specific examples of how some isotopes from Yb to Os can be reached via the *s*-process path only, some via the *r*-process only, and some via both.

far from the stability line, and when they decay from the *s*-process position close to the line, as illustrated in detail in Fig. 1.8. Some isotopes will be shielded from the *r*-process path by a stable isotope on the way, and some isotope positions will be unreachable by the *s*-process path, while some isotopes can be reached both from an *s*-process route and from an *r*-process route. In Fig. 1.8 is illustrated the detailed nuclear path for isotopes of the elements from Yb to Os. It is seen that ^{175}Yb is β -unstable with a decay half-life of $\tau=4.2$ days. This is short enough that the general *s*-process surroundings will not add another neutron before the decay of the ^{175}Yb nuclei to ^{175}Lu . Therefore ^{176}Yb , which is stable, will be an *r*-only isotope. Similarly ^{186}W and ^{187}Re will be *r*-only isotopes, while ^{186}Os will be an *s*-only isotope (the *r*-process element decay is stopped by the stable ^{186}W *r*-process isotope), and ^{187}Os is almost an *s*-only isotope, apart from the very small contribution from the *r*-process by the $\tau=50$ billion years decay of the *r*-only isotope ^{187}Re . It is also seen that ^{176}Hf and ^{180}Ta cannot be reached by either the *s*-process nor the *r*-process. These two isotopes are therefore *p*-process elements. The *p*-process elements are few and rare, as illustrated in Fig. 1.7. We understand from Fig. 1.8 that we in nature will have some isotopes of heavy elements which are pure *r*-process isotopes, some which are pure *s*-process isotopes, some which are pure *p*-process isotopes, and many isotopes which are a mixture of a certain percent *r*-process and a certain percent *s*-process nuclei. Fig. 1.7 show the abundance of the isotopes that are pure *r*-, *s*-, and *p*-nuclei, together with the sum of all nuclei to each mass number atom.

1.6 High- and low-mass stars produce different of the elements

We have now discussed the physical conditions and mechanisms for formation of the different groups of elements: hydrogen and helium, carbon and oxygen, the elements between oxygen and iron, the iron group elements, and the elements heavier than iron. However, we still need to discuss where in nature these conditions prevail. In other words: which types of stars produce the different elements and when during their

evolution ?

In order to do this, we will first introduce the important division line between low-mass and high-mass stars – those that end their lives as white dwarfs, versus those that end as supernovae. Then we will discuss how many there are of each of the two types of stars, and how much processed mass they will return into interstellar space per year, that new stars and planets can form from. Then we will go into a more detailed description of the supernovae and comparison of their predicted nuclear yield with observed abundances. Finally, we will embark into a discussion of how low-mass stars evolve and how they can produce carbon and *s*-process elements and return them into interstellar space without an explosive event.

1.6.1 high-mass stars

Fig. 2.3 in the chapter about supernovae sketch the evolutionary tracks of stars between 9 and 120 times the solar mass. They live all of their lives at very high luminosities – typically 10,000 times the solar luminosity or more – and their total lifetime is therefore very short. As an example, Tab. 1.3 gives the lifetime of a $25M_{\odot}$ star of solar metallicity. Tab. 1.3 also lists the time such a star can sustain its luminosity by various of the nuclear processes discussed in the preceding chapters. We recognize the successive shorter time-scales of burning as the binding energy differences between the reactant and the burning product becomes successively smaller when we approach the iron group elements. We also see that all the nuclear processes discussed in the preceding chapters will take place during the $25M_{\odot}$ star's life. We will see in a coming chapter that this stellar model is (close to being) representative for the important supernova that was seen in the Large Magellanic Cloud in 1987.

Stage	Core temperature	Core density	Duration of stage
Hydrogen burning	40 million K	5 g/cm ³	7 million years
Helium burning	200 million K	700 g/cm ³	700,000 years
Carbon burning	600 million K	200 kg/cm ³	600 years
Neon burning	1.2 billion K	4 tons/cm ³	1 year
Oxygen burning	1.5 billion K	10 tons/cm ³	6 months
Silicon burning	2.7 billion K	30 tons/cm ³	1 day
Core collapse	5.4 billion K	3000 tons/cm ³	1 second
Explosion	≈ 1 billion K		10 seconds

Table 1.3. The time-scales of the nuclear burning processes that will take place in a solar metallicity, $25M_{\odot}$ star.

For those stars that end their lives in a supernova explosion, it is quite obvious how they will return into the interstellar medium the material they have produced during their lives. These stars go through all the nuclear burning processes described in the preceding chapters, so they will contain all the elements from oxygen to iron and return these into the interstellar medium (ISM) during the explosion. They will also produce the *r*-process elements in nature during approximately 1 second of the supernova explosion itself, and these elements will obviously be returned into the ISM with the exploding material as well. We will introduce the two main types of supernovae below, and discuss which elements are produced in each of them, and show that qualitatively a combination of yield from these two types of supernovae can explain approximately half of the existing elements in nature (remark that this simple fact is often misrepresented in popular books, and even in some text books, which give the erroneous impression that all elements are produced in supernovae).

It is not well known how massive a star has to be in order to end in the condition which makes it explode as a supernova. The main difficulty is not in the description of the explosion mechanism, but rather in the description of the convection in the core of stars during their ordinary lifetime, and in calculation of the amount of mass that is lost to space via a stellar wind during the life of a star. The problem with the core convection, is that comparison of evolutionary models with observations of stars, seems to indicate that the core of the stars are generally larger than predicted. This theoretical problem is sometimes fixed by *ad hoc* introducing a so-called overshooting parameter, which determines how far beyond the formal convection

criteria one will still introduce convection in the models. By introducing convection in a larger volume of the central parts of the star than ordinary (mixing length) convection theory prescribes, the core becomes larger than it would have been without overshooting. Since it is the size of the core which determines whether the star explodes as a supernova, less massive stars with overshooting than stars without overshooting will now formally develop large enough core masses to explode as supernovae. Therefore, introducing overshooting, lowers the mass boundary between what we will call low-mass (i.e., which will not end as a supernova) and high-mass (i.e., supernova producing stars). On the other hand, if the star loses a lot of mass via a stellar wind during its life, it will effectively be smaller by the end of its life than if it didn't lose mass. If stars have strong stellar winds some time during their lives, the boundary between low-mass and high-mass will therefore be more toward higher initial mass than if stars have no mass-losing wind. We will return to the discussion of the poorly understood field of mass loss via winds later in connection with how material produced in low-mass stars get to the interstellar medium, but for the moment it will be sufficient to note that there is a boundary between high-mass and low-mass, which may be at $8M_{\odot}$ but which may also be as low as $5M_{\odot}$ or as high as $10M_{\odot}$.

Because $5M_{\odot}$ stars are much more abundant than $10M_{\odot}$, the exact value of the chemical enrichment from supernovae is very dependent on our (lacking) knowledge of the exact value of the boundary mass between low-mass and high-mass stars. The contribution from low-mass stars are, on the other hand, much less dependent on this value, because there are many more stars of $3M_{\odot}$ than of 5 or $8M_{\odot}$, so it is the group of stars with masses below $3M_{\odot}$ ($0.8M_{\odot}$ to $3M_{\odot}$) that contribute with most of the cosmic enrichment from low-mass stars, independent of where exactly the dividing line between low- and high-mass stars is to be drawn.

1.6.2 low-mass stars

The stars we here define as high-mass stars, are those where nuclear processes in the central region of the star proceeds all the way to iron and builds up enough degenerated iron that it will eventually collapse under its own gravity, hereby triggering a supernova explosion. In contrast to this, the low-mass star will not have enough mass to reach high enough temperatures for the final processes toward the creation of an iron core to take place, and it will stop its life as a star (i.e., stop nuclear burning) while it has only completed some of the nuclear processes discussed in the preceding chapters.

Stars with masses in-between the limit between stellar and sub-stellar masses ($\approx 0.08M_{\odot}$, depending on metallicity) and approximately $0.7M_{\odot}$, are the most abundant stars in the Universe, but they will only be able to convert hydrogen to helium. They will never reach high enough temperatures in their cores to initiate the helium to carbon burning reaction, and will, hence, end their lives as helium rich white dwarfs. Since they do not produce elements heavier than helium, they will never contribute to the heavy element enrichment of the Universe. The lifetime of a $0.7M_{\odot}$ is longer than the present age of the Universe, and therefore there exist no stars which have yet (by themselves and without mass loss) evolved to the helium-rich white dwarf stage. All the low mass stars with $M < 0.7 M_{\odot}$ that has ever been born in the universe, still shine as stars that are converting hydrogen to helium.

Stars in the mass range up to about $3 M_{\odot}$ will develop a degenerate helium core, as will be described in detail below, and ignite the helium explosively in their core. It's a "mini-supernova" explosion that takes place when the core helium ignites in these stars (with an explosion energy of $\approx 1\%$ of a real supernova), but it leaves no trace of its existence in the observable spectrum. Stars of about $0.8M_{\odot}$ (and low metallicity) have lifetimes identical to the present age of the Universe, while stars of $3 M_{\odot}$ live about 500 million years. There exist therefore stars today of all masses in this interval, which have evolved through all their nuclear burning phases. These stars will end their lives as oxygen-rich white dwarfs, and they contribute substantially to the enrichment of the Universe with carbon, nitrogen, *s*-process elements, and perhaps selected other nuclei.

Qualitatively the evolution of this group of stars are well represented by the globular cluster stars, and the nomenclature for low-mass stars are therefore adopted from the morphology of globular clusters. We talk about the red giant stars, meaning low-mass stars which are in an evolutionary phase analogue to the one stars in globular clusters are in when they develop up along the red giant branch of the cluster in an HR-diagram (transforming hydrogen to helium in a shell around a helium core). We talk about the (low-mass)

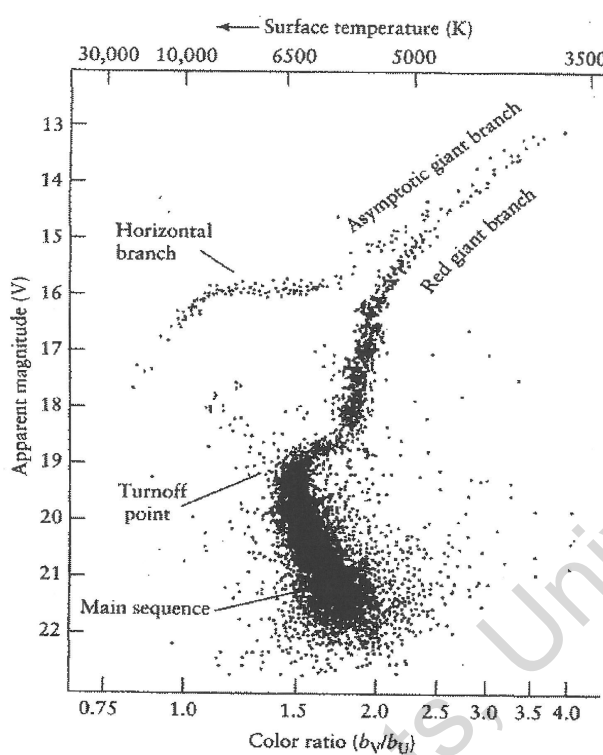


Figure 1.9. The observed HR-diagram of the globular cluster M3.

horizontal branch phase of evolution, meaning when the stars burn helium to oxygen in their cores, just like globular cluster stars do when they populate the region in the HR diagram that forms a horizontal line in the diagram. Finally, we talk about the asymptotic giant branch phase of low-mass stars when they burn helium to carbon and/or hydrogen to helium in a shell around an oxygen core, just like they do in globular clusters while they move upward through the HR-diagram along a line which asymptotically approach the red giant branch in the diagram for cluster stars. For short we call low-mass stars in these evolutionary phases for RGB, horizontal-branch, and AGB stars. The corresponding regions in the observed HR-diagram for the globular cluster M3 is shown in Fig. 1.9.

The post-main sequence evolution is very short compared to the main sequence evolution, and when we observe a globular cluster, we will therefore see post-main sequence stars with basically only one (initial) mass (typically $0.8 M_{\odot}$), but main sequence stars of many different masses, from the post-main sequence value and downward. The morphology of the post-main sequence stars in a globular cluster, is therefore basically identical to an evolutionary track of a star with one specific mass and chemical composition.

The accounting for the half of nature's elements that comes from low-mass stars are in many respects more tricky than accounting for the half that comes from supernovae. We are, however, quite certain where the *s-process* elements come from, but we are much less certain about where nitrogen and carbon (the most central atom in organic molecules !) come from. We will discuss the theory that all these elements are produced in low-mass stars during the final phases of their lives. However, the low-mass stars do not explode, so we will need a longer and more complex description of how we envision the elements are created in the stellar interior, mixed into the outer stellar envelope, and finally blown from the photosphere and into interstellar space in a non-violent fashion, probably via the stellar wind.

1.6.3 The relative contribution of low- and high-mass stars to recycled material.

The relative contribution to the chemical enrichment of the Universe from low-mass and from high-mass stars, is given mainly by three things: (1) The relative number of stars as function of mass, (2) the amount of

mass that is returned to interstellar space compared to the mass that is left in a stellar remnant, and (3) the degree of enrichment of the material that is returned.

The relative number, $dN = f(M)dM$, of stars born per time interval with mass in the interval from M to $M + dM$, can be expressed by the **initial mass function** (IMF) which is a power law of the form

$$f(M) dM = a M^\gamma dM \quad (1.12)$$

normalized such that

$$\int_0^\infty f(M)dM = 1 \quad (1.13)$$

The value of γ has been a much debated issue in the literature throughout the years, and particularly for the very highest mass stars (say, above $50 M_\odot$) and for the very lowest mass stars (say, with mass $M < 0.5 M_\odot$) the value is still very uncertain. Often the value $\gamma = -2.35$ derived by E.E.Salpeter in 1955 (ApJ 121, 161, 1955) is still used. It is simple to use, because it is the same number for all stellar masses. However, it does not reproduce more recent observations. We will here adopt a graduated scale, with γ changing as function of M , such that

$\gamma = -2.5$ for $M > M_\odot$,

$\gamma = -2.2$ for $M \approx 0.5 - 1.0 M_\odot$, and

$\gamma = -1.3$ for $0.08 M_\odot < M < 0.5 M_\odot$.

By substituting these values for γ into Eq. 1.12 it is seen that

$$\int_5^\infty M^\gamma dM / \int_{0.08}^5 M^\gamma dM = 0.01 \quad (1.14)$$

i.e. that only $\approx 1\%$ of the stars born per time unit in our Galaxy have masses above $5 M_\odot$.

We have used here $M = 0.08 M_\odot$ for the lower mass limit of stars, and a bit arbitrarily (due to the non-existence of better knowledge) assumed that the IMF continues from $0.5 M_\odot$ to $0.08 M_\odot$ with the same value of γ .

The number of stars which die per time unit is the same as the number that is born per time unit – for stars with masses above the minimum mass that have had time to develop through its life within the present age of our Galaxy, and provided the IMF is constant in time (which it probably is).

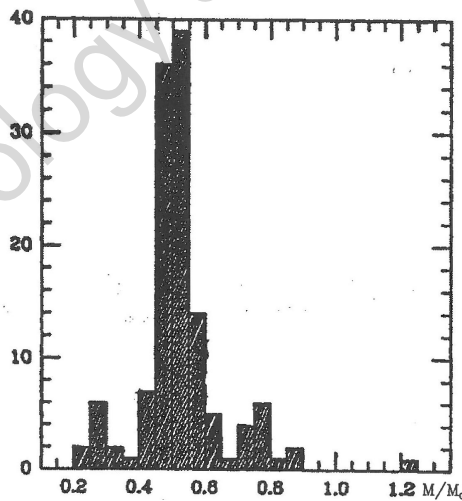
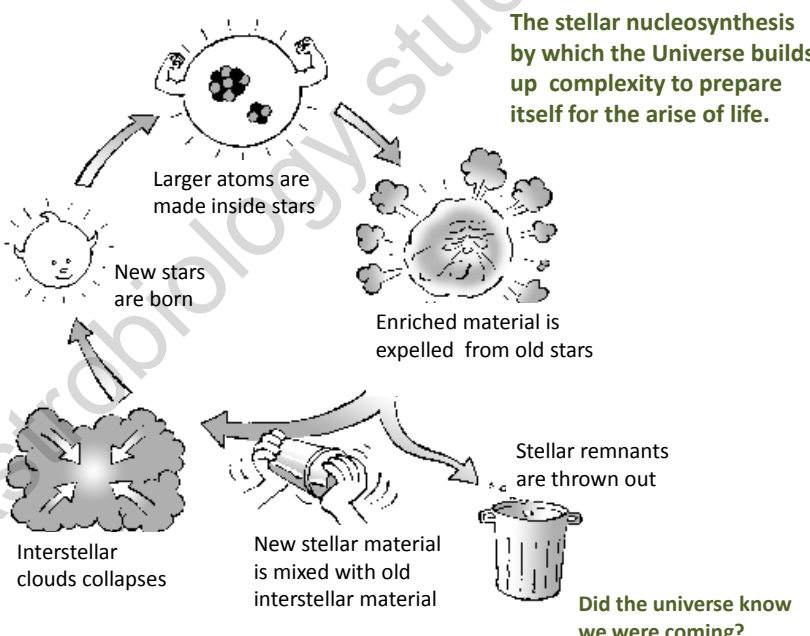


Figure 1.10. The mass distribution function of observed white dwarfs that are not members of multiple systems. Note the strong concentration around $0.55 M_\odot$.

We will leave it as an exercise to show that if the mass division between the stars that do/do-not become supernovae is $5 M_\odot$, then approximately half of the mass that stars expel into the ISM today per time unit

comes from supernovae and about half from low-mass stars, while if the division line is at $8M_{\odot}$, then about one third comes from high-mass stars and two thirds from low-mass stars. For solving this exercise one should use that degenerate iron cores collapses when they are $1.4M_{\odot}$, and the very puzzling fact, illustrated in Fig. 1.10, that almost all single white dwarfs (i.e., those that are not members of a binary system) have a mass very close to $0.55M_{\odot}$. (when solving this exercise one should note that todays mass loss is independent of the stellar population below $0.7M_{\odot}$, and therefore also independent of our adopted γ for the mass range $0.08M_{\odot}$ to $0.7M_{\odot}$. Furthermore one could discuss how the ratio of returned mass from supernovae and from low-mass stars change with time – was it smaller or larger during the early days of our Galaxy's life, and how will it be in the future ?)

We see from the calculation above that the relative number of high-mass stars is very small, and that the amount of mass returned to the ISM from the high-mass stars is not dominating the re-circulation of matter. Nevertheless, the chemical enrichment to our Galaxy from high-mass stars can be much higher than immediately expected from these numbers, because the material returned from the low-mass stars may be dominated by unprocessed hydrogen and helium, whereas the material returned from the supernova explosions may be very rich in newly synthesised nuclei. In praxis, we will see below that probably around half of the mass that has been produced since the Big Bang comes from supernova, while most of the other half of the mass comes from the wind of low-mass stars.



For astrobiology students, Univ.Cph.2023

2

Supernovae

2.1 SNI and SNII – the two main types of supernovae.

Spectroscopically, supernovae are divided into two main groups. Those which show spectral lines of hydrogen in their spectra (called SNII) and those which do not (called SNI). Obviously, type II supernovae must have preserved some of their initial hydrogen in an envelope surrounding the exploding core (as would be the case if the progenitor is a high mass star with a degenerated iron core surrounded by onion type shells with the successive burning processes described in the previous chapter and illustrated in the upper panel of Fig. 2.1), while type I must have got rid of all its hydrogen prior to explosion. The classification is further subdivided according to whether the spectra show Si, He, O, and other elements, as illustrated in Fig. 2.2, and due to the form of the light curve.

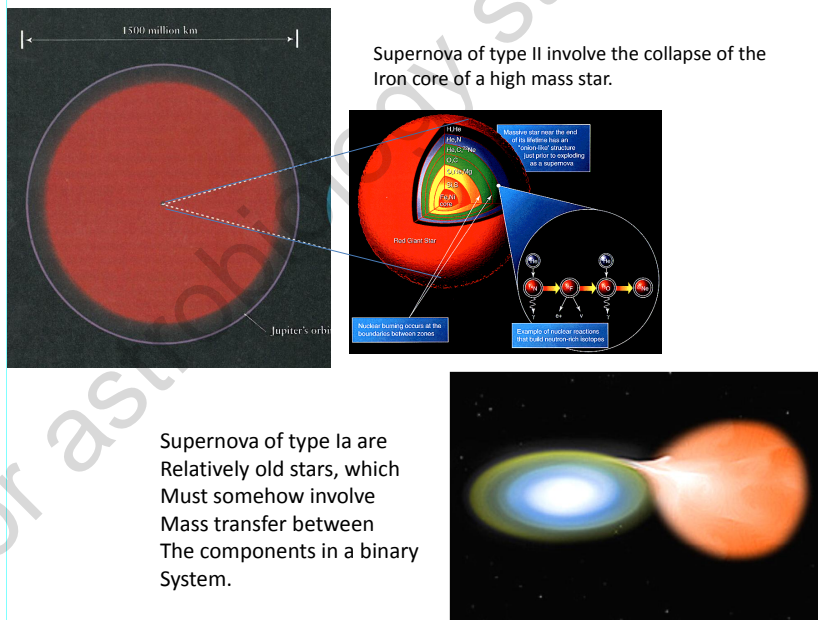


Figure 2.1. Upper panel: The schematic structure of a high mass star shortly before it explodes as a supernova of type II. Lower panel: SNIa must somehow involve mass transfer between stars in a binary system.

SN of type II are mainly associated to the galactic spiral arms. Since stars are primarily born near the inner edge of the spiral arms, and thereafter drift though the arms in relatively short time, it was early realized that SNII are likely to be associated to short-lived (i.e. high-mass) stars, which all later observations and models have only confirmed. Supernovae of type I were originally thought to be associated then to the low-mass stars, because they were more evenly distributed inside the spiral galaxies and among galaxies. This simple picture has later turned out to be likely to be completely wrong, and it is now common to divide the SNI into at least 3 different spectral classes (as is illustrated in Fig. 2.2), which most likely have completely different physical origin.

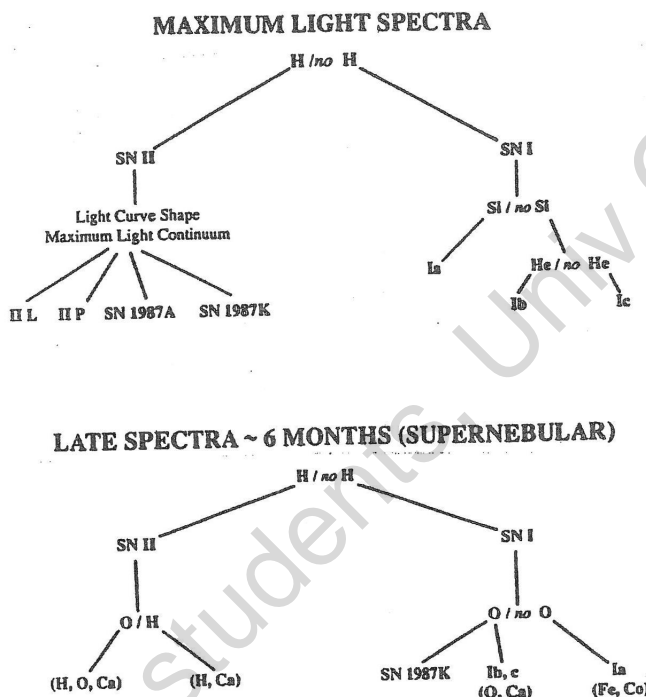


Figure 2.2. The spectroscopic classification of supernova, from their spectra at maximum light, and from their spectra ≈ 6 months later.

Systematic surveys of galaxies and clusters of galaxies reveal several new supernovae every month, and from these surveys we know that approximately half of all supernova explosions are of type II, approximately one forth are of type Ia, and another one forth are of type Ib or Ic. The rate of supernova explosions seen in galaxies of the same type as our own, make us believe that the Milky Way has a rate of approximately 4 supernovae per century, so we should expect a new SNII every 50 years and a SNIa per 100 years in our galaxy. Nevertheless we know of only 7 historical supernovae during the last 1000 years.

We attribute this lack of observed Galactic supernovae to the obscuring effect of the large interstellar clouds. Of the 7 historical supernovae, it seems that 3 were of type Ia, namely both Kepler's and Tycho Brahe's as well as a supernova recorded in 1006.

The most well understood of the supernova types is SNII. Its progenitor is a single star with an initial mass above the critical mass dividing the white dwarf producing stars from the supernova exploding ones. All the nuclear burning processes described in the previous chapter will take place right until a core of iron is produced in the center, as illustrated in Fig. 2.1. When the mass of this core exceeds $1.4 M_{\odot}$, it will implode (i.e., collapse). When the pressure is getting high enough electrons penetrate the columb barrier of protons in the iron nucleus, transforming them to neutrons, hereby reducing the electric repulsion between the iron nuclei. The transformation of the whole $1.4 M_{\odot}$ core from iron to neutrons take of the order of 1 second. During this time the core implodes down to ~ 10 km size. The neutrinos produced when the protons plus electrons are transformed to neutrons will exert a tremendous pressure on the remaining gas overlaying the

imploding core, which together with a shock wave created by gas bouncing on the neutron surface, will lift the overlaying gas layers off in an explosion. When the expanding gas masses have implanted their movement to the surface layers approximately 1 day after the core collapsed, we see a (visual) supernova explosion. The first rise we see in the luminosity (i.e., the explosion) is due to the increased size of the expanding surface and due to the heating of the gas. Later we will see energy created from decay of produced ^{56}Ni to ^{56}Co ($\tau_{1/2}=6.6$ days) and further to ^{56}Fe ($\tau_{1/2}=77$ days) from deep down in the gas.

2.2 SN1987A played an important role for our good understanding of supernovae of type II

The most detailed knowledge we have about supernovae of type II is from SN1987A, which was seen exploding in the large Magellanic cloud in February 1987. It was the first supernova seen with the naked eye since the historical supernovae observed by Tycho Brahe in 1572 and by Johannes Kepler in 1604. Since the telescope was invented in 1606, it is also the first very bright supernova which we have had the opportunity to observe with a telescope. Obviously the amount of detailed knowledge we have about SN 1987A is tremendously much larger than the information we have about any other supernova. Although it was not inside our own Galaxy, but in the neighbouring galaxy the Large Magellanic Cloud (LMC), it was close enough for its progenitor to have been studied before the explosion. Fig. 2.3 shows the HR-diagram of the brightest stars in the LMC, with the arrow identifying the star Sanduleak $-69^{\circ} 202$ which later exploded as SN 1987A.

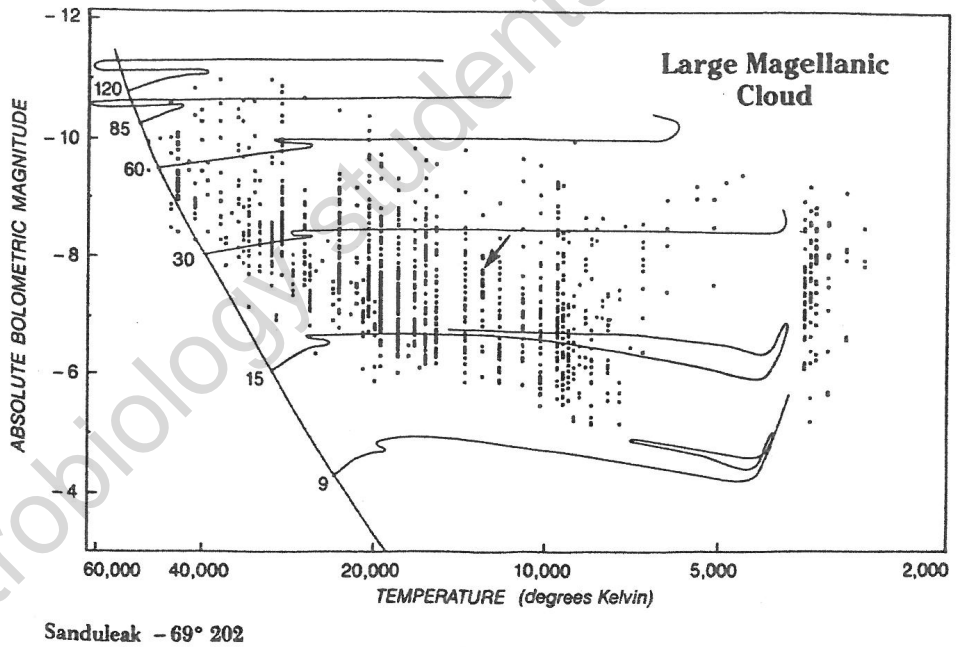


Figure 2.3. The effective temperature versus luminosity diagram for the brightest stars in LMC, shown together with the theoretical zero-age-main sequence and the evolutionary tracks of stars with initial masses of 9, 15, 30, 60, 85, and $120 M_{\odot}$. The arrow identifies the star Sanduleak $-69^{\circ} 202$ which exploded as SN 1987A.

The (bolometric) light curve for the first 1/2 year after the explosion is seen in Fig. 2.4 upper right panel together with the calculated form of the light-curve if the energy (after ≈ 50 days) came from decay of $0.14 M_{\odot}^{56}\text{Co}$ and from $0.07 M_{\odot}^{56}\text{Co}$, respectively. Also shown in this panel is the lightcurve as it would have looked like (with a sharp drop in intensity during the second month after the explosion) if there were no

energy input from radioactive ^{56}Co at all. It is seen that the observed light-curve is in good agreement with $0.07 M_{\odot}^{56}\text{Co}$ being produced during the explosion. After the initial increase in luminosity due to expansion of the hot gas (and the following decrease due to successive dilution of the gas), the energy for the light comes from the radioactive decay of ^{56}Co to ^{56}Fe . The upper left panel of Fig. 2.4 shows the light curve over a somewhat longer period of more than 2 years following the explosion, and it is seen that the logarithm of the luminosity falls off linearly with time, with a half life which is exactly the half life of the decaying ^{56}Co (77 days). It was predicted that after some weeks the radioactive cobalt would come close enough to the surface that x-rays from the decay would be able to escape directly to space through the overlaying envelope. The "light"curve of this x-ray energy was measured by x-ray satellites as shown in the lower part of the upper left panel of Fig. 2.4. The x-rays were actually visible a bit earlier than predicted, which lead to a refinement of the traditional picture of a spherically symmetric expansion of the gas, to a more detailed understanding involving instabilities leading to fingers of interior material breaking its way through toward the surface from the interior, as illustrated in the lower left panel of Fig. 2.4. At the same time the spectral line of ^{56}Co was appearing in the spectrum, and slowly decaying away over the following months. In the lower right panel of Fig. 2.4 is shown a piece of the spectrum showing the ^{56}Co line as it appeared on November 12, 1987.

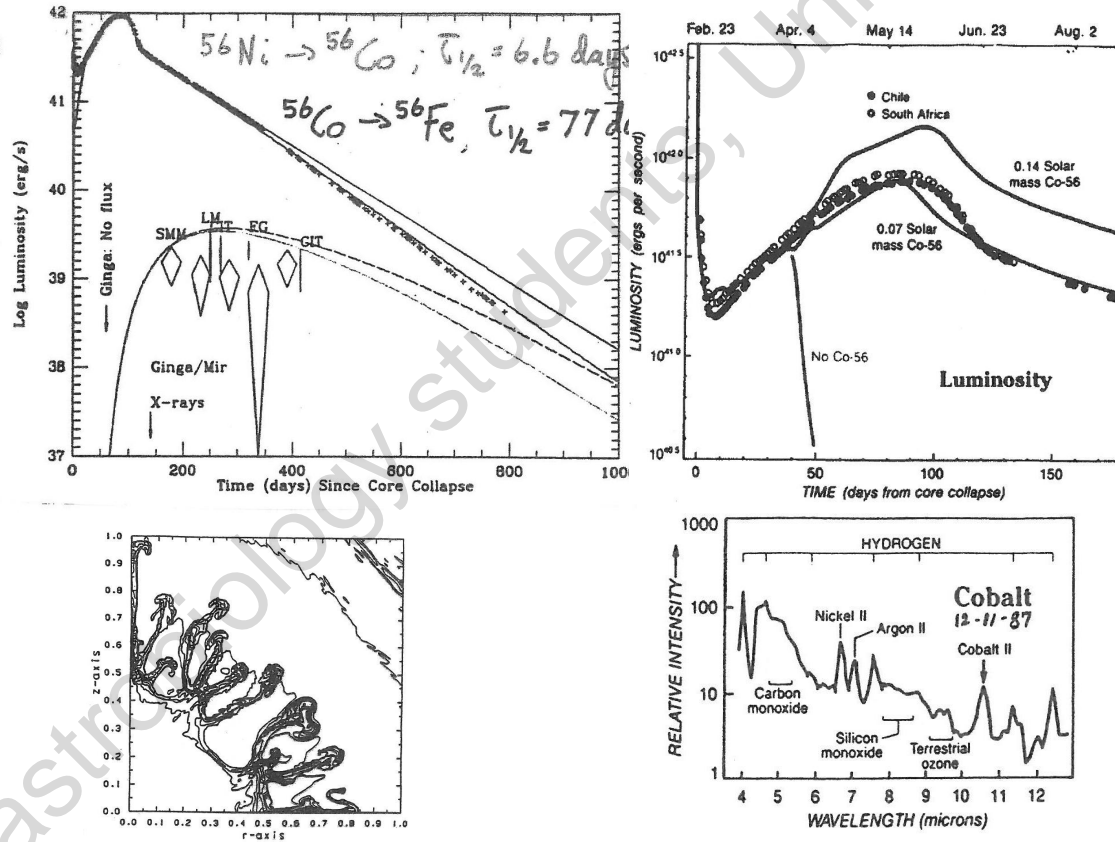


Figure 2.4. The bolometric luminosity of SN 1987A during the first 175 days (upper right panel) and first 800 days (upper left panel), respectively. Also shown in the upper right panel are three different predicted light curves under the assumptions of: (1) no radioactive cobalt produced during the explosion, (2) the production of $0.07 M_{\odot}^{56}\text{Co}$, and (3) of $0.14 M_{\odot}^{56}\text{Co}$. In the lower right panel the spectrum of SN 1987A on 12/11/87 from 4 to $13 \mu\text{m}$, shows among other lines the ^{56}Co line at $10.5 \mu\text{m}$. The energy from the decay of ^{56}Co give rise to the perfect linear decay of the logarithm of the luminosity shown in the upper left panel, as well as the development in observed X-ray luminosity as measured from various satellites and shown in the same panel. The observed X-ray structure forms the basis of the refined explosion model illustrated in the lower left panel.

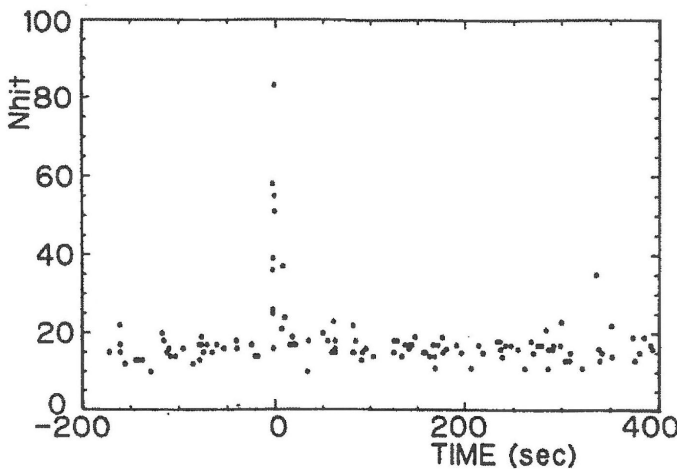


Figure 2.5. The number of neutrinos measured in Kamiokande during the seconds around the core collapse of SN 1987A. Beside the excess in numbers of neutrinos close to $t = 0$, also the energies of these neutrinos are larger than the energies of the background neutrinos seen during the rest of the shown period.

Collision of a high energy electron with a proton will transform the proton to a neutron and an electron neutrino, at the rate of one neutrino per collision. Models of supernovae of type II predict that a driving force of the explosion is the huge amount of neutrinos produced during the ultra-short collapse phase of the $1.4M_{\odot}$ stellar core, when electrons collide with protons in the iron nuclei that makes up the stellar core. In complete agreement with the predicted number from our understanding of the SNII core collapse theory, a total of 24 neutrinos were detected in the 3 existing detectors at that time – 11 at the Japanese Kamiokande detector, 8 in the Cleveland detector in USA, and 5 neutrinos at the Baksan Neutrino Observatory in Russia. The neutrinos registered in the Kamiokande neutrino detector is shown in Fig. 2.5.

It is quite amazing that numerical models have been able to simulate the detailed burning processes in stars that will lead to the formation of the elements most of our nearby surroundings are made of (ourselves, the biosphere, and the Earth itself), the formation of a degenerate iron core in high mass stars, and the detailed final collapse of this core involving complicated physical processes we can only reproduce in the most powerful accelerators in the world, forming the almost undetectable and somewhat mysterious neutrino particle – and yet SN1987a showed us that exactly the number of neutrinos predicted from such simulations were produced in this violent stellar explosion. After having traveled through empty space since before the first humans left Africa, 24 of these neutrinos were finally detected in the first neutrino detectors, shortly after they were switched on for the first time.

The neutrinos arrived simultaneously at the three detectors (which are all in the northern hemisphere, and hence the neutrinos have traveled through the Earth before being captured by the detectors), three hours before the first observed visual glimpse of the explosion. If the neutrino rest mass is zero, they would travel with the speed of light, and the arrival time between the neutrinos and the first visible light would correspond to the time it takes for the hot gas from the interior of the exploding star to be swirled to the surface (which is expected to be of the order of one day). If the neutrino mass was on the large end of the theoretically estimates, the neutrino burst would have arrived after the first light glimpse, and if the neutrinos would travel with the super-light speed inferred from the neutrino experiments in Italy during 2013, then the neutrinos would have arrived a year or more before the first light glimpse. SN 1987A therefore also gave us firm limits on the neutrino mass, which showed that its mass is not exactly zero, but very small, in fact smaller than was speculated to make it a candidate for the dark matter and/or energy.

The event of SN1987A was a tremendous triumph for confidence in our ability to quantitatively model (and hence understand) the basic physics that leads to the collapse of the iron core in a high mass star and the following supernova explosion of type II. This fact of course also leads to some confidence in our ability to model the nucleosynthesis in SNII, although we should not forget that the relative role of SNII in the production of the various elements in nature, depends on the distribution of SNII from stars of many different initial masses (of which not all of them are as well understood as the one that lead to SN1987A),

and in particular on the role of mass loss via a stellar wind long time prior to the explosion, which is a subject not very well modeled yet. Scientists are now eagerly waiting for the next supernova of type II to explode in our own galaxy, and existing detectors are now online reporting their measurements to a central computer, SNEWS, at Brookhaven National Laboratories, where a time coincidence of less than 10 seconds between several detectors in the world will trigger an automatic alert to observatories around the world that a supernova might be seen exploding within hours in a certain direction of the sky (at present with an accuracy of a few degrees). Detectors under construction or just ready, such as the south polar Icecube experiment, the Japanese super-Kamiokande, or the Italian Borexino, will be able to detect thousands of neutrinos if the explosion is somewhere inside our own Galaxy, and in a high time resolution that will allow to judge for example whether the stellar core collapsed into a black hole (leading to an abrupt end of the neutrino burst) or a neutron star (leading to a gradual fade out of the burst over a few seconds). The two last super novae observed in our Galaxy were both of type Ia, and dates more than 400 years back, and yet we expect from observations of other galaxies similar to the Milky Way that a couple of type II super novae explode per century – so statistically we could expect the next “nearby” supernova and associated large neutrino burst to be “any day” in the near future.

2.3 The origin of SNI is not as well understood as type II

While the level of understanding of SNII must be said to be very good, this cannot be said about the type I supernovae. Common to all the type I supernovae is that they have no hydrogen in their spectra, but this may not mean that their origins have anything in common, and type IA, IB, and IC are today believed to represent 3 different explosion causes and mechanisms. The SN Ib and SN Ic are the least well understood. Most likely they are due to the explosion of extreme high-mass stars which have lost their hydrogen envelope prior to explosion. It is generally believed that the SN Ia explosion is caused by mass transfer onto a white dwarf, whereby it exceeds a mass limit (the Chandrasekhar limit) where it explodes under its own gravitation. We will limit our discussion below to the case of white dwarf explosions, i.e. to type Ia's.

One obvious way of transferring mass onto a white dwarf, would be if it was a member of a binary system, where the other component was losing mass that could be captured by the white dwarf. If SN Ia are really caused by such mass transfer we should be able to identify mass transferring stellar systems which could be considered progenitor systems. The major types of such systems are (1) symbiotic stars, (2) novae, and (3) cataclysmic variables.

Symbiotic stars refer to a general class of relatively widely separated binary stars, where one component loses mass via a wind and the other component captures a fraction of this material. Typically this could be a red giant losing mass to a white dwarf, but it could also be for example a B-star losing mass to a neutron star hereby emitting X-rays. The process is relatively inefficient to transfer mass, and it is therefore not the most likely candidate for the SN Ia progenitor.

Novae are objects which on time-scales of a few hours increase typically 8 mag. (i.e., more than a factor 1000) in luminosity. Most likely they represent the explosive ignition of approximately $10^{-4} M_{\odot}$ material which has been accreted onto a white dwarf. Traditionally it has been believed that novae could be the progenitors of supernovae of type Ia, because one could envision that the nova explosions gradually converted the accreted hydrogen-rich material on the surface of the white dwarfs to helium and possibly further, hereby slowly bringing the white dwarf above the Chandrasekhar limit of $1.4 M_{\odot}$, where it would explode as a SN Ia without any trace of hydrogen in the spectrum.

There are about $5 \cdot 10^{-10}$ nova eruptions per pc^3 per year in the solar neighbourhood, which corresponds to approximately 100 novae per year in the entire Galaxy ($5 \cdot 10^{-10} (30 \text{ kpc})^2 150 \text{ pc}$). Since a typical (single) white dwarf is very close to $0.55 M_{\odot}$ (see Fig. 1.10), we would need to add almost $1 M_{\odot}$ to a typical white dwarf in order to bring it up to the explosive Chandrasekhar limit. If of the order of $1 M_{\odot}$ is to be dumped onto the white dwarf and each nova eruption is of $10^{-4} M_{\odot}$, a given mass accreting white dwarf must give rise to of the order of 10^4 nova eruptions during its “nova phase of life”, indicating that we would expect that approximately one white dwarf would end its nova phase per $10^4 [\text{eruptions/wd}] / 10^2 [\text{novae/year}] = 100 [\text{years/wd}]$, meaning that every 100 years a new nova would have finished (or begun) its nova phase. This is approximately the same as the SN Ia rate, giving support to the idea that after 10^4 nova eruptions over 10^8

years, a white dwarf has accreted material enough to explode as a SNIA.

However, theoretical computations indicate that a large fraction, if not all, of the $10^{-4} M_{\odot}$ ignited material is blown off from the white dwarf during the nova explosion. Furthermore, observations often show very strong CNO (i.e., carbon, nitrogen, and oxygen) lines in the spectra of novae, which most likely has to be interpreted as showing that not only the accreted $10^{-4} M_{\odot}$ hydrogen and helium is blown off during the explosion, but also a small piece of the existing (carbon and oxygen-rich) white dwarf itself. In this way it seems difficult to get the white dwarf increase in mass toward the Chandrasekhar limit. On the contrary it instead seems that the net effect will be a decrease in mass during the accretion period. We will see a possible way out of this dilemma below, but here only stress that it for the moment is difficult – theoretically as well as observationally – to understand how a white dwarf will be able to increase its mass due to accretion of material.

Besides the classical novae described above there are other classes of novae, the most important being (1) the **dwarf novae** which behave like classical novae in many respects, but increases only 2 to 5 mag. during the eruption instead of the 8 mag. typical for classical novae, and (2) the **nova-like variables**, which have never been seen in eruption, but which show variability very similar to what is often seen in stars before they erupt as classical novae. Finally the so-called **slow novae** are systems which seems to be in a nova-explosion like stage continuously for years. It is believed that these are symbiotic systems where the white dwarf accreted material slow enough that it is actually burned steadily to helium at a high rate instead of exploding.

Cataclysmic variables (CVs) are close binary systems with orbital periods typically from a few hours to a few days. Here one component (typically a white dwarf) is receiving mass from a donor star which typically is a main sequence star. As oppose to the symbiotic variables where the mass transfer is via a wind, the mass transfer in CVs are via Roche lobe overflow. The orbital periods in the CV systems can be as short as $P_{\min} = 10$ minutes (for helium stars, and 80 minutes for hydrogen stars). Obviously some breaking of the orbital movement must have taken place. It is envisioned that first the largest of the two component grows to fill its Roche lobe, such that mass is flowing onto the lower mass component (left panel of Fig. 2.6). When enough mass has flown onto the smallest star till it also fills its Roche lobe, no mass can flow from one star to the other in the system, but instead mass is flowing from both stars out into a common envelope (right panel of Fig. 2.6). The drag force on both components due to their movement in the common envelope reduce the orbital separation. Further decrease of the orbital period can eventually be caused by magnetic braking and by gravitational radiation when the orbit becomes small enough (lower panels of Fig. 2.6).

A detailed study of planetary nebulae has shown that approximately 10% engulfs not only one white dwarf in its center, but two white dwarfs orbiting one another with a period shorter than one day. These must have been cataclysmic variables just before the slowest evolving of the two components became a white dwarf and corresponding planetary nebula. From studies of white dwarfs we know that there are about 10^{-2} per pc^3 . Hence, we should expect a density of $\approx 10^{-3} \text{ pc}^{-3}$ of binary systems that at some stage during the life-time of our Galaxy has been through the CV phase. The scale height of the CVs are ≈ 150 pc, and the total number of CVs that have been in our Galaxy must therefore be

$$N_{CV} = (30 \text{ kpc})^2 150 \text{ pc} 10^{-3} \text{ CVs}/\text{pc}^3 = 150 \text{ million CVs} \quad (2.1)$$

If the age of the Galaxy is of the order of $t_{gal} = 10^{10}$ years, the birthrate, F_{CV} , (\equiv the death rate) of CVs is

$$F_{CV} = N_{CV}/t_{gal} = 10^8/10^{10} = 10^{-2} \text{ CVs per year} \quad (2.2)$$

i.e., that \approx one CV is expect to end its life per 100 years in our Galaxy, which is identical to the rate of SNIA.

We are therefore now ready to propose the theory that classical novae are white dwarfs in a cataclysmic variable which accreted material from the other component in the system, whereby it over a period of probably 10^8 years will increase its mass beyond the Chandrasekhar limit and explode as a supernova of type Ia.

I have already mentioned the problem with this theory that it seems, both from numerical models and from observations, that the accreted material on the white dwarf is blown into interstellar space during the nova explosions. In-spite of this complication, the theory may be the best one presently available for explaining SNIA, and it may even be the correct one. We will now discuss conditions under which we may be can come around the accretion-explosion problem.

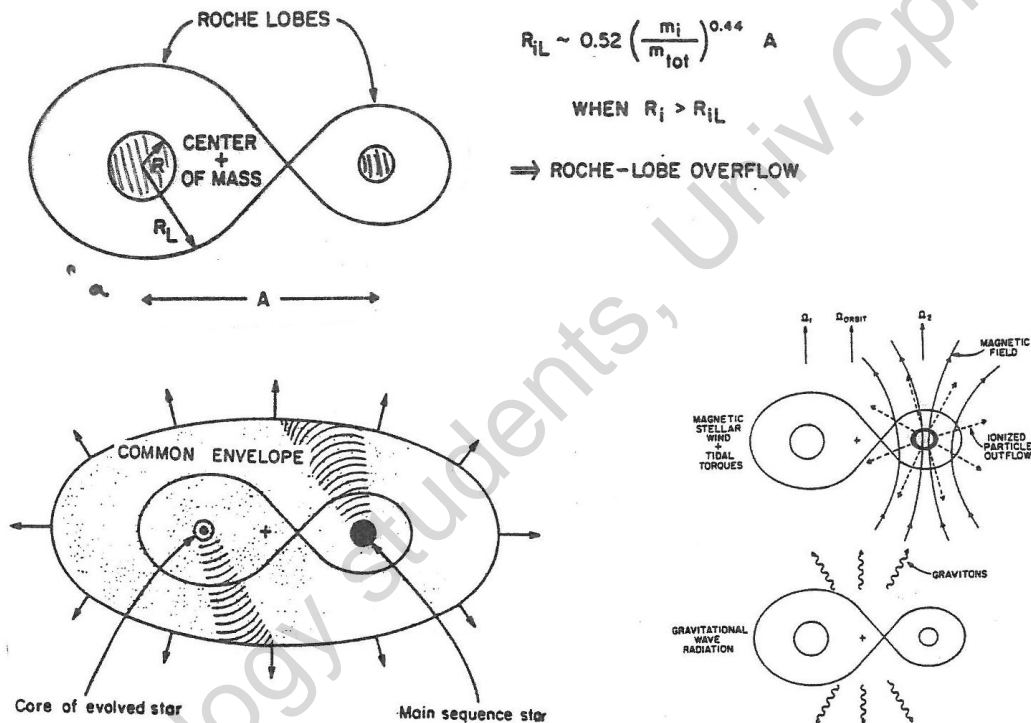


Figure 2.6. Four stages of the creation and evolution of a cataclysmic variable: (1): The highest mass component in a close binary expands to fill its Roche lobe, such that material is finally flowing onto the lower mass component. (2) The low mass component hereby grows to a size such that also it fills its Roche lobe. Material now cannot flow from one star to the other, but instead flows from both stars into a common envelope and out of the system. The orbital separation shrinks due to drag force on the two stars when they move through the common envelope. (3) The orbits can eventually shrink further due to magnetic breaking and gravitational radiation.

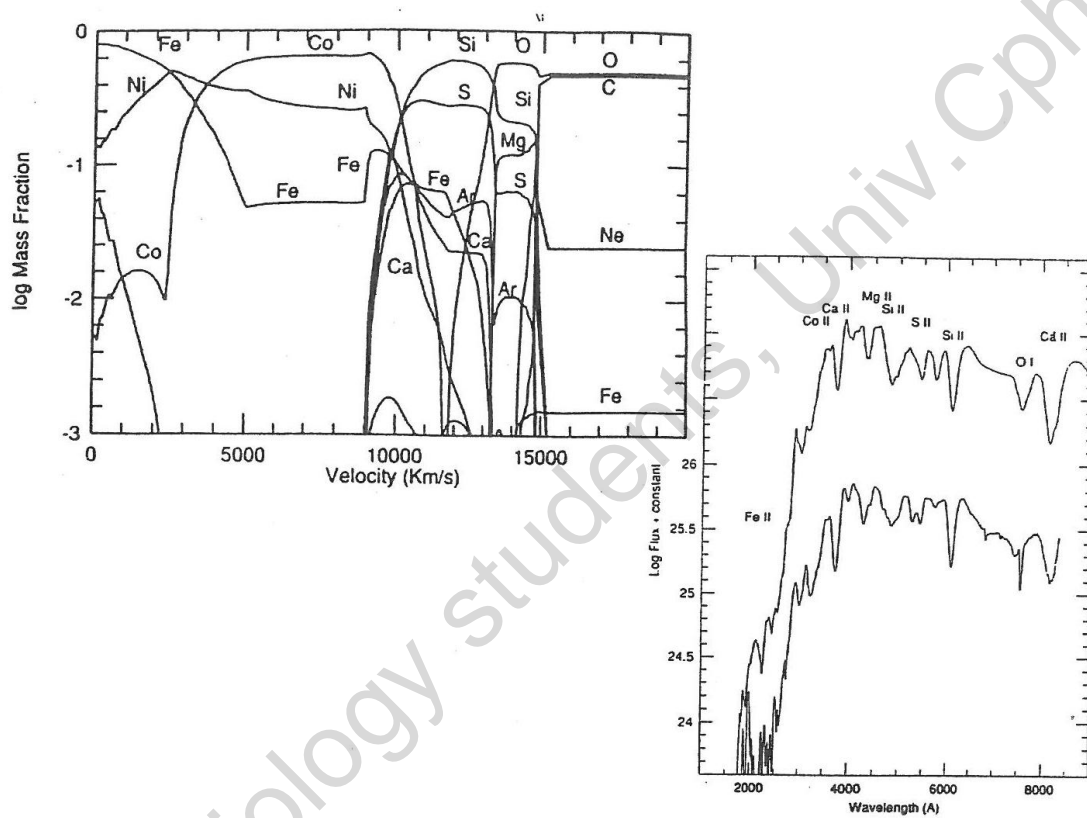


Figure 2.7. Upper (left) panel shows the composition as function of the velocity of the outflowing material produced by a model of a thermonuclear deflagration in a carbon-oxygen white dwarf two weeks after the explosion. Lower (right) panel shows the good agreement between the spectrum of the SNIA SN1981B and the synthetic spectrum based on a corresponding deflagration SNIA model.

From a numerical modeling point of view, it has turned out that the evolutionary scenario of the accreting white dwarf is very dependent on the accretion rate, \dot{M} , with the following 4 different scenarios as outcome:

(1): $\dot{M} \leq 10^{-9} M_{\odot}$ per year:

Since the mass distribution function for single star white dwarfs is a very narrow distribution around $0.55 M_{\odot}$, a typical white dwarf will have to accrete $0.85 M_{\odot}$ of material before it reaches the $1.4 M_{\odot}$ required to explode as a supernova. With an accretion rate of $10^{-9} M_{\odot}$ per year, the required accretion will take a minimum of 0.85×10^9 years. In reality we will expect a substantially larger time because a large fraction of the material accreted seems to have to be blown off during the nova explosions. The time-scale for build up to the Chandrasekhar mass is therefore uncomfortably large if the mass accretion rate is this low. However, the kind of supernova explosion we end up with from this slow accretion is a so-called deflagration, which is the only one that produce a supernova spectrum (and hence elemental yield) in agreement with observed SNIA spectra.

(2): $10^{-9} < \dot{M} < 5 \times 10^{-8} M_{\odot}$ per year:

Accretion rates in this range will lead to detonation of the C-O white dwarf core and the He envelope, which means that nuclear burning during the explosion would have to proceed to its equilibrium value, which is in disagreement with the observed compositions inferred from SNIA spectra.

(3): $5 \times 10^{-8} < \dot{M} < 10^{-6} M_{\odot}$ per year:

Helium will burn non-degenerately during this high accretion rate, resulting in SNIA progenitors, which should be so bright that we would easily see quite a number of them with the naked eye in the night sky (which is not the case).

(4): $\dot{M} \geq 10^{-6} M_{\odot}$ per year:

Accretion of this rate is faster than the hydrogen can manage to burn, which would result in the presence of hydrogen in the SNIA spectrum, in contradiction with observations.

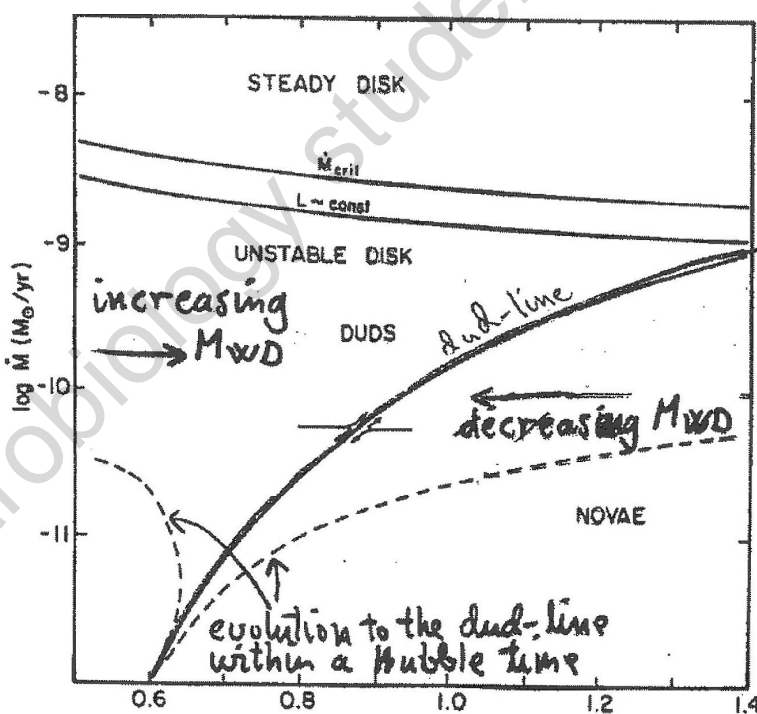


Figure 2.8. The nova dud-line in an accretion rate \dot{M} versus white dwarf mass diagram. White dwarfs to the left of the dud-line will increase their total mass as a result of accretion, while WD's to the right of the dud-line will lose mass as a net result of the accretion. For accretion rates increasing with time a WD can develop up along the dud-line, while decreasing accretion rates will result in development down along the dud-line. Dashed lines show the locations from which it will take a Hubble time to reach the dud-line.

If we for the moment disregard the slow evolution toward the SNIA explosion caused by the very low accretion rate of $\dot{M} < 10^{-9} M_{\odot}$ per year, then seemingly we can create the right type of SNIA explosion if we can get the material to accumulate on the surface of the white dwarf until a large enough mass has been accomplished. When we claimed above that it is impossible for models to keep the accreted material on the surface of the white dwarf, it is a truth with a little bit of modification. The modification is that if the mass of the white dwarf is small enough the accretion will actually lead to accumulation of material on the surface of the white dwarf as a result of the accretion (which is of course at first not interesting, because we are looking for WDs toward the Chandrasekhar limit). Only when the mass is above a critical mass will the accretion lead to a decrease of the total mass (i.e., more than the accreted material will be erupted during the nova explosion). The value of the critical mass depends on the accretion rate (below $10^{-9} M_{\odot}$ per year). The line formed by these combinations of critical mass and accretion rates is called the nova dud-line, and it is shown in Fig. 2.8. It is seen that if the accretion rate is steadily increasing it will actually be possible to cross back and forth over the nova dud-line in such a way that mass is slowly accumulated on the white dwarf (while for decreasing accumulation rate the white dwarf mass is decreasing), and hereby evolve toward the Chandrasekhar limit – although uncomfortably slow compared to the age of our Galaxy.

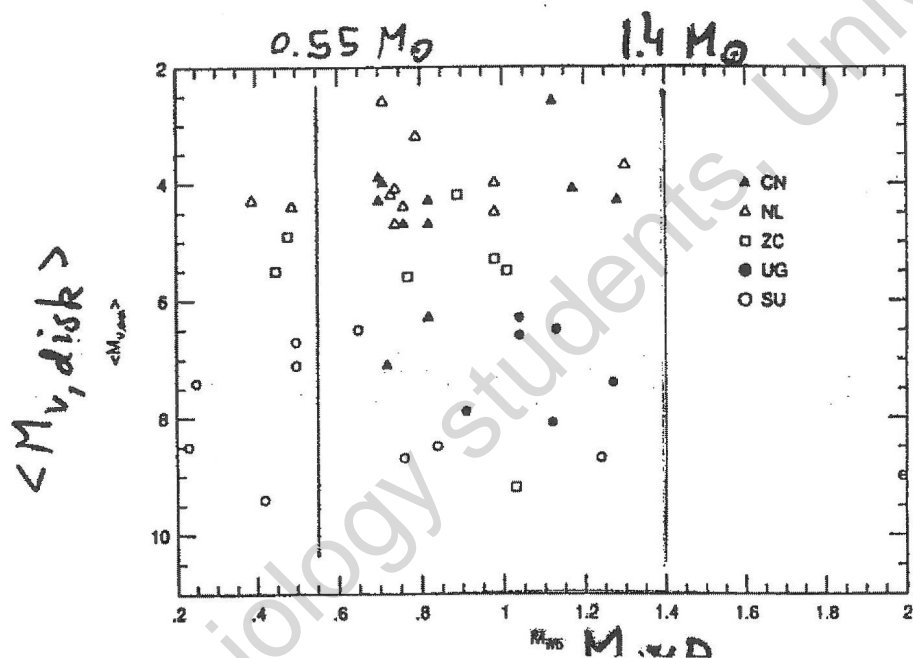


Figure 2.9. For systems of an accreting white dwarf surrounded by an accretion disk, is here shown the absolute visual magnitude of the disk versus the mass of accreting white dwarf. The magnitude of the disk is a measure for the accretion rate. It is seen that the mass distribution function of the white dwarfs in such systems is very flat compared to that of single white dwarfs, and extends all the way up to the Chandrasekhar limit at $1.4 M_{\odot}$.

That this kind of mechanism may contain some level of reality is indicated in Fig. 2.9, which for white dwarfs surrounded by an accretion disk, shows the luminosity of the disk as function of the mass of the accreting white dwarf. The luminosity of the disk (and hence the visual magnitude $\langle M_{v,disk} \rangle$ given along the axis) is almost identical to the luminosity L_h of the hot spot at the interception where the mass from the Roche lobe of the secondary flows over onto the disk. L_h can be expressed as

$$L_h = \frac{GM\dot{M}}{R_{disk}} \quad (2.3)$$

Hence, the y-axis of Fig. 2.9 basically indicates the accretion rate, while the x-axis shows the mass of the

white dwarf. It is seen that on the average these accreting white dwarfs (independent of the accretion rate) have much higher mass than the single white dwarfs shown in Fig. 1.10, and that their mass distribution is almost flat up to the Chandrasekhar limit, in strong contrast to the mass distribution for single white dwarfs.

We conclude that there is some indication that SNIa could come from accreting white dwarfs although we admittedly are not fully able to account quantitatively for how the accretion of material could take place at short enough time-scales. Before possibly accepting the theory completely, we further have to discuss another serious problem of the SNIa–CV theory. We could call it "the missing naked-eye observations of abundant SNIa progenitors".

In order that the spectrum of the SNIa can be without hydrogen lines, the accreting hydrogen needs to be converted at least to helium. For every gram of hydrogen which is converted to helium we have already seen that we gain

$$\Delta mc^2 = \frac{4m_H - m_{He}}{4m_H} c^2 = 7.2 \cdot 10^{-3} g (3 \cdot 10^{10} \text{ cm/s})^2 = 6.5 \cdot 10^{18} \text{ erg/g}_H \quad (2.4)$$

If $0.85 M_\odot$ were to be accreted, of which 70% was hydrogen, the energy release would be

$$E_{\text{accretion}} = 0.7 \cdot 0.85 \cdot 2 \cdot 10^{33} \cdot 6.5 \cdot 10^{18} = 7.7 \cdot 10^{51} \text{ erg} \quad (2.5)$$

The fastest possible burning rate is at the Eddington luminosity (the limit above which the material will blow off due to radiation pressure on the gas), $L_{Edd} = 10^{38}$ erg/s. I.e., the hydrogen burning energy cannot be released in a shorter time scale than

$$t_H = E_{\text{accretion}} / L_{Edd} = 7.7 \cdot 10^{51} \text{ erg} / 10^{38} \text{ erg s}^{-1} = 7.7 \cdot 10^{13} \text{ s} = 2.4 \cdot 10^6 \text{ years} \quad (2.6)$$

If the SNIa rate of one per 100 years in our Galaxy shall be explained by accreting WDs in CVs, we will at any given time have at least

$$N_{\text{accreting-WD}} = t_H / R_{SNIa} = 2.4 \cdot 10^6 \text{ years} / 100(\text{years/SNIa}) = 2.4 \cdot 10^4 \text{ SNIa} \quad (2.7)$$

In other words, we will in our Galaxy at any given time have at least $2.4 \cdot 10^4$ SNIa progenitor accreting white dwarfs shining at the Eddington limit. If we assume a lower burning rate than the Eddington limit these objects will be dimmer, but we will have even more of them. The area of our Galaxy is approximately $30 \cdot 30 \text{ kpc}^2 = 900 \text{ kpc}^2$, so that within 1 kpc in all directions we would expect

$$N_{\text{progenitors}} = 4 \cdot 2.4 \cdot 10^4 / 900 = 100 \quad (2.8)$$

Using the basic definitions of the relations between luminosity (L/L_\odot), absolute and apparent bolometric magnitudes (M_{bol} and m_{bol}), and distance (D), we find that these accreting objects will be brighter than

$$\begin{aligned} m_{bol} &= M_{bol} + 5 \log(D) - 5 = M_{bol}^\odot - 2.5 \log(L/L_\odot) + 5 \log(1000) - 5 \\ &= 4.75 - 2.5 \log(10^{38} / 3.9 \cdot 10^{33}) = -6.3 + 10 = +3.7 \end{aligned} \quad (2.9)$$

In other words, we should expect that 100 of the bright stars easily visible with the naked eye in the sky should be such hydrogen burning SNIa progenitors. However all the brightest stars are very well studied, and none of them are this kind of objects.

Due to the many problems with what we could call the SNIa-nova-WD-CV theory it was suggested some years ago that the progenitor of a SNIa is instead the result of the merging of two white dwarfs. This would also fit with the counting we did above based on binary WDs inside planetary nebulae, if a mechanism could be found to shrink the orbit of these after the (second) planetary nebula phase. The model suggested that gravitational radiation could transport away the necessary amount of orbital energy to allow the two WDs to merge. This still needs to be proven, and it is also needed to quantify a mechanism which would make the merger of the two white dwarfs explode below the Chandrasekhar limit (since obviously $0.55 M_\odot + 0.55 M_\odot = 1.1 M_\odot < 1.4 M_\odot$). The authors of the theory envisioned that the shock wave from the merging itself could trigger a deflagration in the object in-spite of its too low mass.

Although there are obviously many problems in explaining the SNIA, it seems hard for the moment to envision anything else than some mechanism evolving a white dwarf that due to more or less sudden increase in its mass up to a limit close to (or at) the Chandrasekhar limit will make it start a deflagration. It, however, also seems very likely that we will need to modify the theory in some or several respects. Which modifications is needed is a question to be solved one day by some of the bright students at Copenhagen University now following a course on the nature of supernovae and related topics.

2.4 Elements from oxygen to iron are dominated by supernovae yield

After this discussion of the supernovae of type II and Ia we are now ready to return to the discussion of the elements produced in the supernova progenitors and during the supernova explosion itself, and the supernova yield, i.e. the rate at which new elements are introduced into the interstellar medium by supernovae, such that new stars and planets can be created from them.

TABLE I. Yields per Star (Solar Masses)

$M(\alpha)$	M	He	C	O	Ne	Mg	SiCa	Fe
2.7	10.0	0.90	0.048	0.004	0.000	0.000	0.000	0.020
3.0	12.0	1.52	0.048	0.004	0.000	0.000	0.000	0.030
4.0	15.0	2.04	0.192	0.167	0.040	0.066	0.101	0.050
6.0	20.0	2.58	0.288	0.774	0.426	0.254	0.265	0.070
8.0	25.0	3.10	0.568	1.660	0.767	0.270	0.339	0.100
12.0	31.0	3.59	1.220	3.840	1.040	0.311	0.424	0.140
16.0	39.0	4.06	1.620	6.160	1.420	0.405	0.979	0.190
24.0	55.0	5.02	2.300	11.700	1.980	0.624	0.934	0.240
32.0	85.0	8.62	2.050	16.800	2.350	0.970	1.190	0.300

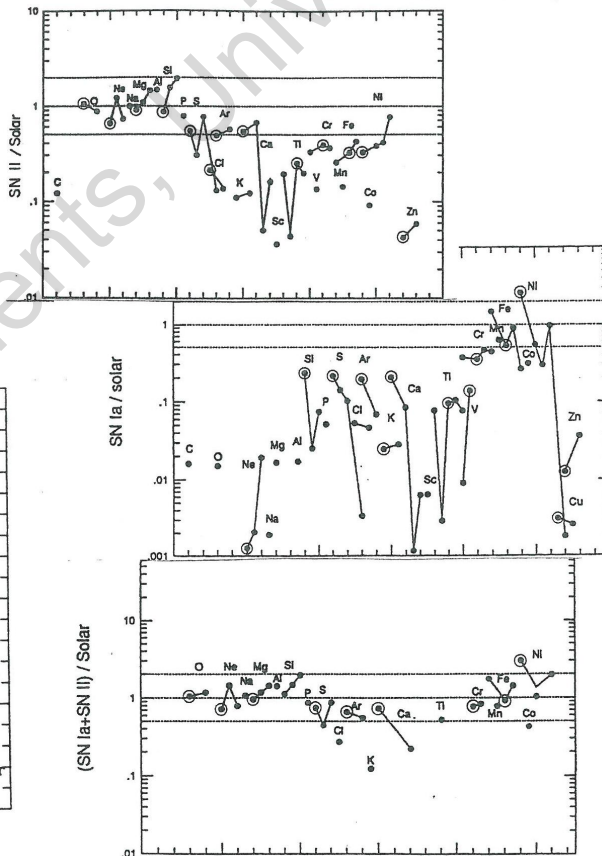
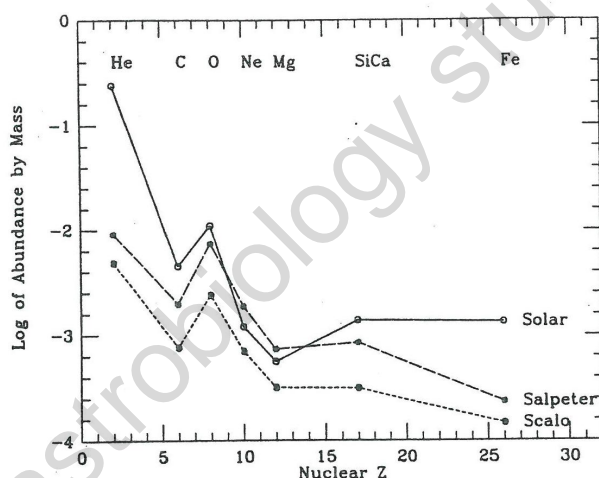


Figure 2.10. Upper left panels: The yield of selected elements from stars of various initial masses. Lower left: The solar abundance of elements from He to Fe, compared with the total composition of yields from SNII assuming an IMF following respectively Scalo's and Salpeter's formulas. Upper right panel: The yields from SNII relative to the solar abundance. Middle right panel: The yields from SNIa relative to the solar abundance. Lower right panel: The combined yields from a ratio of 1:10 of SNII:SNIa.

Fig. 2.10 compares the relative abundances from helium to iron in the solar photosphere with the relative abundances from a combination of supernova explosions of type II. The calculated yield from supernovae of

stars with various masses are given in the accompanying table to Fig. 2.10. The combined yield from all these supernovae of course depends on the relative number of stars with each of the listed masses. This relative occurrence is expressed in the initial mass function, IMF, as described in detail in connection with Eq. 1.12 to 1.14 in the previous chapter. The two curves marked Scalo and Salpeter represent the relative combined SNII yield one would get by adopting an IMF due to each of those two authors. In both cases it is seen that there is a relatively good agreement between the SNII results and the solar abundance for the elements from oxygen to silicon. Note that the abundance scale is logarithmic, such that for example the discrepancy for carbon corresponds to that only approximately 20% of the carbon in nature can have been produced in supernovae of type II, only 10% of the iron, and only 2% of the helium.

Fig. 2.10 show again (in the upper right panel) the average SNII yields, but now normalized to the relative solar abundances, such that a straight line $y = 1$ would correspond to that the relative yields were the same as the relative solar abundances. The lines above and below this line represent a factor of 2 above and below, respectively, the relative solar abundances. The middle panel shows the corresponding yields from a type Ia supernova. It is seen that the two yields complement one another well, indicating the elements from oxygen to silicon are mainly produced in supernovae of type II, while the iron group elements could be produced in SNIA. The lower right panel in Fig. 2.10 show the relative yields obtained by combining the SNII and SNIA yields in a ratio of 1:10. Of course we do not expect to have the supernovae II and Ia in the ratio 1:10, but rather in the ratio 1:2, but the exercise clarify how the two abundance patterns complement one another, and qualitatively it indicates that the elements from oxygen all the way through the iron group may have been produced in a combination of various types of supernovae.

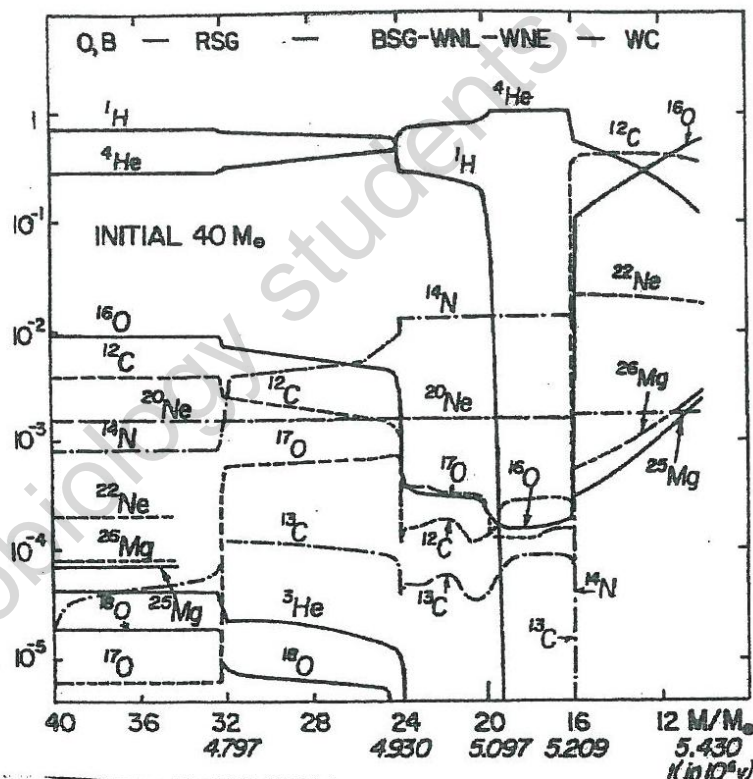


Figure 2.11. The development from an initial $40 M_{\odot}$ O,B stellar model to a $12 M_{\odot}$ WC type Wolf-Rayet star, due to mass loss over a period of 5.43 million years. Curves show the relative surface abundance of various elements that will be ejected with the wind.

Although the above may give the impression that we have good agreement between the supernova yields and the solar abundances, I will rush to illustrate that the problem definitely is complicated enough to include major surprises yet from several generations of scientists wanting to involve themselves in this important

field of research. Fig. 2.11 shows one simulation based on our present day limiting understanding of the mass loss phenomenon. The figure shows the surface composition of a mass loosing initial $40 M_{\odot}$ star, and hence the relative abundance of the material that is blown into space as a function of time. From left to right in the diagram the star evolves from a $40 M_{\odot}$ (lower x-axis) O,B (upper x-axis) star to a $12 M_{\odot}$ WC star (Wolf-Rayet C-type star). A WC star is a hot high-mass star which show no trace of hydrogen in its photosphere (spectrum), but often is surrounded by a dense carbon dust envelope. Below the lower x-axis are given numbers from 4.797 to 5.430 (million years). These are the time since the star was born as a zero-age main sequence star. In other words, this model has evolved all the way from the left to the right in the HR-diagram in only 5 million years, while it has lost $28 M_{\odot}$ of constantly changing composition. Five million years old it will explode as a supernova with no trace of hydrogen in its spectrum – maybe a SN Ib. The yield of these stars of course also have to be included into the abundances in Fig. 2.10, but it is still far too complicated and uncertain. Also of course mass loss from the regular SN II have to be taken into account; both concerning the enrichment of the interstellar medium by the stellar wind prior to the supernova, and also concerning the changes in yields compared to the table in Fig. 2.10.

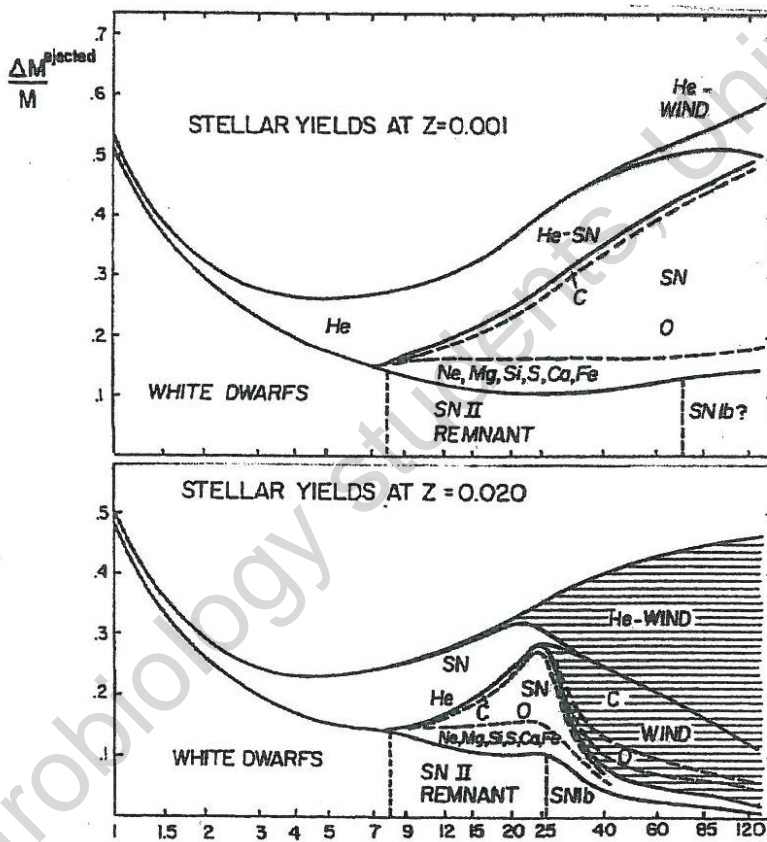


Figure 2.12. Estimates of the total yield returned to the interstellar medium from wind as well as explosion of stars of all initial masses between 1 and $120 M_{\odot}$, as well as estimates of the relative masses of the compact stellar remnants. Upper panel corresponds to computations for $Z=0.001$, while the lower panel shows results for stellar models of solar metallicity, $Z=0.02$.

Fig. 2.12 shows the results of one attempt to calculate the total yield from the stellar wind of all types of stars with initial mass between 1 and $120 M_{\odot}$. The initial masses are listed along the x-axis, while the fraction of the initial mass lost via the stellar wind or ending up in the remnant is indicated along the y-axis. The two parts of the panel show stars of low metallicity ($Z=0.001$) and of solar metallicity ($Z=0.02$), respectively. For example the calculation predicts that a $4 M_{\odot}$ low-metallicity star will end creating a white dwarf of $0.75 M_{\odot}$,

and loose $0.07 M_{\odot}$ He, while a $60 M_{\odot}$ solar metallicity star will loose $25 M_{\odot}$ of nucleosynthesized material via the wind, mainly in the form of He, C, and O, before it explodes as a supernova of type Ib.

In conclusion, concerning nucleosynthesis in supernova, it seems likely that most of the elements from oxygen to silicon may come from supernovae of type II. We understand how these elements are produced in the interior of high-mass stars, and we understand how they get out into the ISM through the SN explosion. Numerical models are able to produce these light elements in roughly the solar relative abundances. All this give us confidence in believing that the elements from oxygen to silicon we find in nature, have their origin in SNIa. We do not understand the origin of supernovae of type I, but models involving (too) slow mass transfer to a white dwarf, does create a deflagration-explosion which completely disrupt the white dwarf and give rise to an emergent spectrum in reasonable agreement with observed spectra of SNIa – the most common type I supernova. The yield derived from observed spectra of SNIa is complementary to the yield from SNIa, in the sense that it shows relatively little oxygen to silicon, but substantial amounts of iron group elements. We therefore believe that the iron group elements in nature is dominated by atoms which were produced during the SNIa explosion of a white dwarf. Due to the complementarity between the elements produced in supernovae of type IA and type II, we are confident that some combination of type I and type II supernovae will be able to explain the cosmic (i.e., solar) abundance of the elements from oxygen to iron. By mass these elements account for a bit more than half of all the material in the Universe which is not hydrogen or helium. The other half is mainly carbon and nitrogen. The origin of these two very abundant and central elements is not yet well known. We will discuss in the next chapter a likely origin of them in the evolution of low-mass stars, but we have also seen in the end of this chapter that WC stars may contribute substantial amounts of carbon to nature.

Among the elements heavier than iron, the r-process elements are believed to form during the seconds of the supernova explosion itself, because this is the only event in nature we know of where neutron densities and temperatures are high enough to make it possible to create these elements. The r-process elements accounts for approximately one third of all the elements (isotopes) heavier than iron. It demands huge amounts of energy to create the elements heavier than iron, and one can with some right say that nature stores some of the energy from the supernova explosion for later release. For example uranium and thorium is created in this process, and during their radioactive decay over biological time-scales following the supernova explosion which created them, they have participated in heating the crust of the Earth, maybe forming an essential basis for the continuing existence of life on our planet. Among the more "peaceful" r-process elements are the precious metals – gold, silver, platinum. Also these are for sure created during supernova explosions, and any person with gold in the teeth, are literally biting on remnants of a supernova explosion.

The other two thirds of the elements heavier than iron are the s-process elements. These are created at lower temperatures and neutron densities than those that were responsible for the r-process elements. We are quite confident that the s-process elements are created during the thermal pulses in low-mass stars during the end of their evolution, in a process that also create substantial amounts of carbon, as to be described in detail below.

3

Low-mass stars

3.1 The evolution of low-mass stars.

In relation to the formation of the elements, the most relevant classification of the stars, is into two groups: High-mass stars and low-mass stars. High-mass stars are those that end their evolution as supernova (of type II and possible some of the other sub-types too), while low-mass stars are those that end their life as white dwarfs. We have seen that a fraction of the white dwarfs can later become supernovae too (of type Ia). The exact mass number of the division line is uncertain due to relatively large uncertainties in our knowledge of convection and mass loss processes. Solving these issues is an important problem in stellar astrophysics with implications for many aspects of astrophysics, but here we will only focus on the fact that there is a division line, and disregard for the moment that we are a bit in doubt about where it is.

The physics behind the division into low-mass and high-mass stars, is whether they are able to reach high enough central temperatures to convert nuclei all the way up to the most stable atom (iron), or whether the process stops before iron. Apart from the division line between high-mass and low-mass stars, there is also an important internal division line inside the low-mass regime, which divides stars that ignites helium explosively (called the helium core flash; "an unseen mini-supernova") at the tip of the red giant branch from those that ignites it non-explosively. Some people call only those that ignite explosively for low mass stars, and the other ones for intermediate-mass stars. The lowest mass stars include the globular cluster stars, and the obvious basis for the terms RGB, HB, and AGB as described in an earlier chapter, therefore are strictly inspired from the morphology of the evolution of the lowest mass stars. In order to get a better feeling for the nucleosynthesis in low-mass and intermediate-mass stars, we will present a short outline of the evolution of a $1 M_{\odot}$ star and a $5 M_{\odot}$ star. The numerical values are taken from the work of J.Lattanzio, 1995, who finds the division line between low-mass and intermediate-mass stars at $4 M_{\odot}$, and the division line to high-mass stars at $9 M_{\odot}$. The $1 M_{\odot}$ and $5 M_{\odot}$ models presented here are therefore truly low-mass and intermediate-mass stars, respectively.

3.1.1 The evolution of a $1 M_{\odot}$ (\sim "truely" low-mass) star.

Figure 3.1 present the computed evolutionary track of a $1 M_{\odot}$ model in an HR-diagram with stellar effective temperature along the x-axis and luminosity along the y-axis. At point 1 in the figure, the model reaches the zero-age-main sequence, ZAMS (i.e., the place where stable conversion of hydrogen to helium in the center of the star for the first time becomes its energy source). During the rest of the star's main sequence evolution, the region where hydrogen is burned ("the core" of the star) becomes larger and larger until the point (point 4 = "the turn-off") where all the hydrogen is exhausted in the center of the star. Due to the

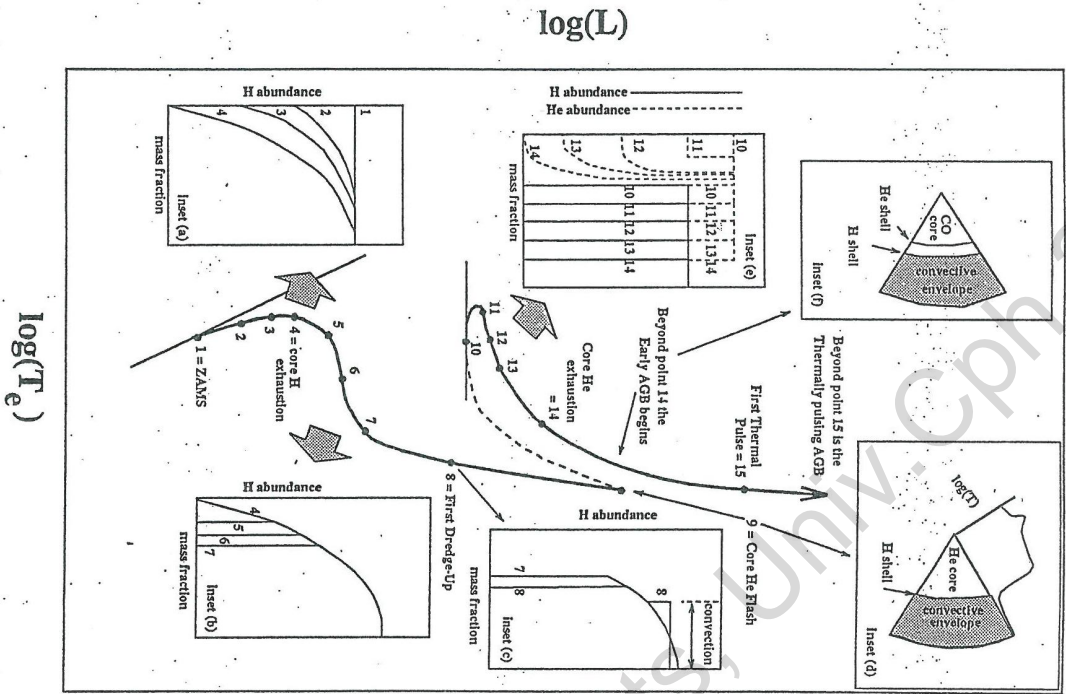


Figure 3.1. Schematic presentation of the evolution of a $1 M_{\odot}$ star.

termination of the energy production in the center, the star readjust to burning hydrogen in a more and more narrow shell around the non-burning, growing, helium core. This part, point 4 to 7, is usually called the sub-giant-branch evolutionary phase. At point 7 the hydrogen burning shell has become very narrow, and therefore moves relatively quickly outward in the star, which makes the star shine brighter, which requires faster nuclear consumption and therefore makes the shell move even quicker outward, etc. The movement up along the red giant branch (RGB, point 7 to 9) is therefore an accelerating process, and the stellar luminosity and the speed of movement depends in a relatively simple way on the mass of the core (i.e., the position of the hydrogen burning shell in mass coordinates), and can be expressed as an analytical function of the core mass alone, almost independent of the total mass of the star and its chemical composition.

For our own Sun the evolution from point 1 to 7 will take 11.5 billion years, whereas the rest of the evolution up along the RGB, HB and AGB will take only 600 million years in total. The evolution up along the RGB is faster and faster as the hydrogen burning shell gets more and more shallow, so most of the time at the RGB is spent at the lower end. Fig. 3.2 show the final 200 million years of the solar evolution, until it reach the planetary nebula phase 12.1 billion years old. The different curves in the figure are based on different models from the literature based on different codes and values on the parameters that describes the microphysics of the final dust formation and corresponding mass loss process. It is seen that depending on the details of the dust formation mechanism, the Sun will either engulf the Earth or expand to a size that is marginally one AU in radius during its very final years on the tip of the AGB, 7.5 billion years from now.

When the energy production in the center increases, the temperature gradient outward through the star steepens, and as a consequence, the convective envelope must penetrate deeper and deeper into the star. This is the same as when you boil a pot of porridge on the stove. When the temperature at the bottom increases, convective movement starts appearing in the porridge in order to transport the energy faster toward the surface. At point 8 in Fig. 3.1 the convective envelope penetrates passed the maximum outer reach of the nuclear burning core during the main sequence (at point 4). Therefore nuclear waste from the core CNO process is now brought up to the surface, in what is called *the first dredge-up*. Since the hydrogen burning

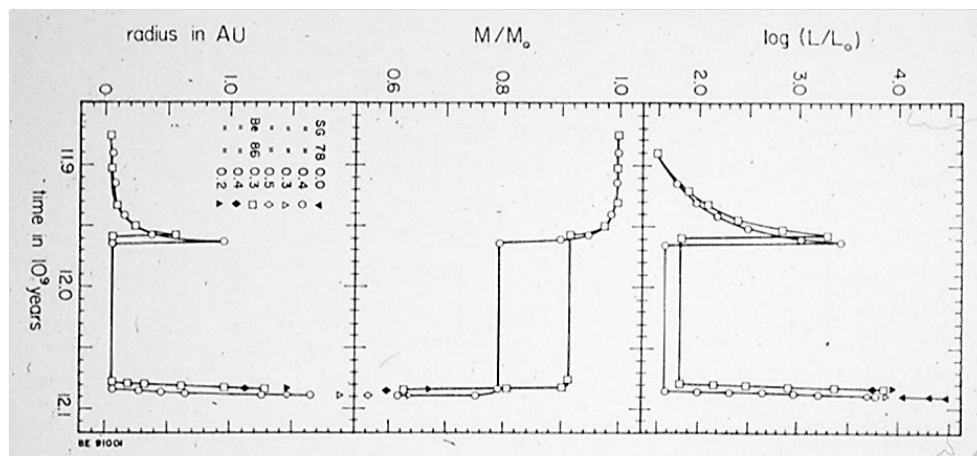


Figure 3.2. The evolution of luminosity (right panel), mass (middle panel), and radius (left panel) of the Sun during its final 200 million years from the RGB over the HB phase to the AGB.

toward the end of the main sequence evolution takes place via the CNO process (Fig. 1.2), the material that is being mixed up during the first dredge-up is enriched in ^{13}C and in ^{14}N relative to ^{12}C , and the resulting stellar surface composition (the one one can see in the stellar spectrum) is therefore expected to decrease in its $^{12}\text{C}/^{13}\text{C}$ and $^{12}\text{C}/^{14}\text{N}$ ratios, toward the CNO burning equilibrium values explained in Tab. 1.2. In reality, such a change in composition is seen appearing already substantially before point 8 (some times already close to point 4), and seemingly details in the theory doesn't quite fit, although the overall picture is probably correct, since we do see more or less the described spectral changes along the RGB. Most of the nitrogen in our body (and surroundings) may come from these processes.

When the helium core mass of the star has reached a specific value, the central temperature will have become high enough for helium to burn to carbon via the triple α process (Eq. 1.7). For low-mass stars the physical conditions in the stellar core is such that the (helium) gas at this place is degenerate. This means that the gas density is determined by the Pauli exclusion principle, and therefore independent of temperature. When the helium ignites, the density will not decrease, as it would have been the case if the gas had followed f.ex. the ideal gas law. With a higher temperature, the nuclear burning will increase, which will cause an even higher temperature, that will cause an even higher nuclear burning rate, etc. The energy production will end up increasing to explosive values before the degeneration will finally be lifted and the star will restructure itself to a structure where the core material is no longer degenerate, and the helium burning can continue in a stable fashion in the core region. The restructuring will bring the star from point 9 to 10 in the figure during such a short timescale (probably a few thousand years) that it has never been observed.

When the star reaches point 10 it is called a zero age horizontal branch (ZAHB) star, and an evolution very similar to the hydrogen burning evolution from point 1 to 7, will now bring the core-helium burning horizontal branch star from point 10 to 14. A difference from the point 1 to 4 evolution is that at point 10 to 14 helium burns to carbon (and further to oxygen via the reaction described in Eq. 1.8), and in addition hydrogen burns to helium (giving rise to most of the luminosity during this phase) in a shell around the helium burning core. When helium is exhausted in the stellar centre (just as for the hydrogen in point 4), an outward moving helium burning shell (Eq. 1.7) will establish itself in-between the hydrogen burning shell and the carbon-oxygen core left by the core helium burning (Eq. 1.7 and 1.8) during the horizontal branch evolution. This phase of shell burning evolution will bring the star moving upward in the HR diagram along a line that is asymptotically approaching the RGB branch, and therefore is called the asymptotic giant branch evolution, or AGB. In the early phase of this evolution, sometimes called E-AGB for early AGB, the two shells are burning simultaneously, but later they have to alternate in a complicated pattern of thermal pulses that give rise to one of the most important nucleosynthetic events of the stellar evolution. This phase is not called late AGB, but TP-AGB to emphasize the central importance of the *thermal pulses* that give rise to the nucleosynthesis during this phase. Since it is rather complex, and common to the low-mass and intermediate-

mass stellar evolution, we will postpone the description of the TP-AGB phase to after having described also the intermediate-mass stellar evolution up to this phase.

3.1.2 The evolution of a $5 M_{\odot}$ (\sim intermediate-mass) star.

The bulk of the intermediate-mass stellar evolution is very similar to that of the low-mass stellar evolution, as is sketched in Fig. 3.3. The core hydrogen burning is more rapid (point 1 to 4) than for the corresponding phases of the low-mass evolution (giving rise to a higher luminosity and a shorter main sequence life time). As a result of the corresponding higher central stellar temperature, more hydrogen is ionized, which result in higher opacity and convective mixing throughout the core region, and therefore a constant hydrogen to helium region throughout the core at any given time (see inset (a) in Fig. 3.3).

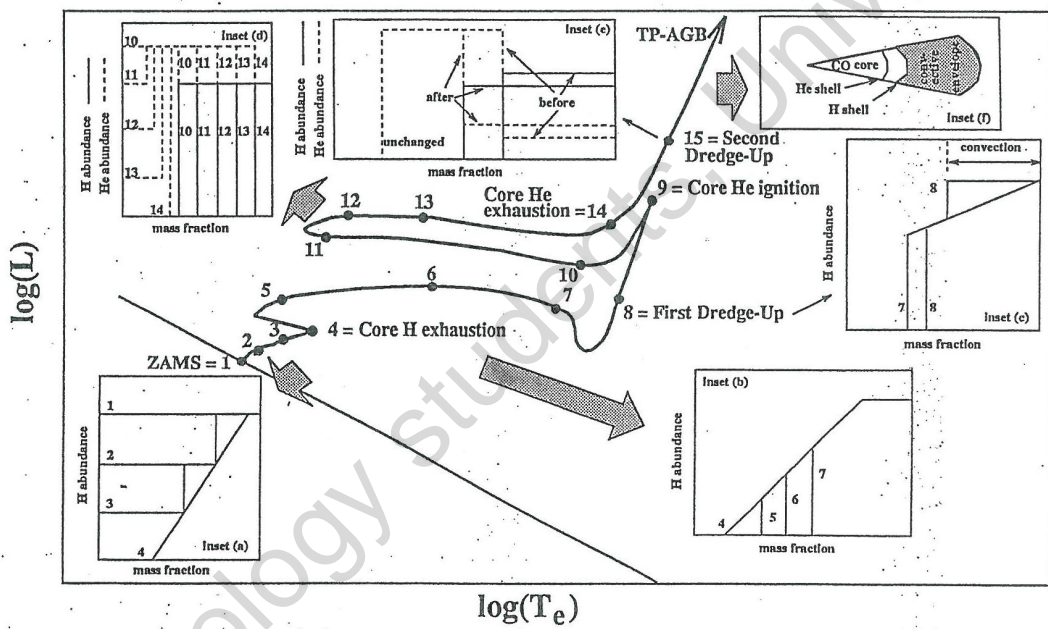


Figure 3.3. Schematic presentation of the evolution of a $5 M_{\odot}$ star.

As more and more hydrogen is converted to helium, which has a higher ionization energy, the abundance of free electrons (and hence the opacity) decreases, and the convective nuclear burning zone therefore gets smaller and smaller, and the surface temperature decreases during the main sequence lifetime, with “a reversed turn off” point (i.e. a minimum MS T_{eff}) compared to the low mass stars where the TO corresponds to the maximum MS T_{eff} . The structural changes upon core hydrogen exhaustion is more substantial than for the low-mass stars, but the short sub-giant (point 4 to 7) and red giant evolution (point 7 to 9) is qualitatively similar to the corresponding evolution for the low-mass stars, including the appearance of the first dredge-up at point 8.

At point 9 (i.e., the red giant tip; RGT), however, the evolution is quite different. For the low-mass stars ($< 4 M_{\odot}$) the (non-burning) helium core was electron degenerated at point 9, but for intermediate mass stars it is described by the non-degenerate equation of state. This means that there will be no explosion and rapid re-adjustment of the stellar structure. Instead the ignition of core helium at point 9 will be accompanied by an expansion of the gas in the core, which will lead to a relatively slow, non-explosive re-adjustment of the stellar structure from point 9 to 10. At point 10 the star will have established a quiescent helium burning

core surrounded by a hydrogen burning shell. The competition of the two energy sources is responsible for the movement on the horizontal branch from point 10 to 14, where stars of these masses are observed as Cepheid variables. At point 14 the helium in the whole convective core region is exhausted, which is accompanied by such substantial re-adjustments and expansions of the star, that the hydrogen burning shell switches off and the outer convective envelope expands downward beyond the former hydrogen burning zone. The accompanied mixing of material from this region to the surface, is called *the second dredge up*. The convective outer zone moves downward in the star and dredges up nucleosynthesised material from the interior for the second time in the star's life. This second dredge up episode takes place only for intermediate-mass stars (not for low-mass stars). Note the slightly confusing notation that low mass stars have only a first and a third dredge-up (while intermediate-mass stars more logically have a first, second, and third dredge-up episode. As we will see below, it is the third dredge-up episode which is the most important for astrobiology and the enrichment of the ISM with nucleosynthesised material. After material has been mixed to the surface, the hydrogen shell burning switches on again, and soon after the star experiences its first helium shell flash, and enters the TP-AGB phase, which is qualitatively identical for stars of all masses in the low- and intermediate-mass regime, and will be described below.

3.1.3 The thermal pulse AGB (TP-AGB) phase of stellar evolution.

About half of all the heavy elements that surrounds us in nature, are created during the thermal pulse AGB phase of low-mass and intermediate mass stars. By the end of the TP-AGB phase the colour of the stars have changed so much, due to chemical reactions involving the newly produced elements, that the changes become clearly visible even to the naked eye. It is more than 100 years ago that the dramatic changes in the stellar spectra were recognized, but it is only during recent years that it has become clear how the new elements are produced and mixed into the spectrum forming regions of the star and further into interstellar space. Although the process is rather tricky, we will describe it here in some detail, due to its enormous importance for the enrichment of the universe with a large fraction of all the elements that surrounds us.

While the hydrogen shell burns its way outward through the star, it obviously leaves behind it an increasing layer of helium. During the TP-AGB phase, the physical conditions in the upper layers of the stars are such that this helium will become hotter and hotter, until it finally ignites semi-explosively in the lower region of the helium shell. The ignition will cause the layers above, where the hydrogen was burning, to expand and cool enough that the hydrogen burning will terminate. After some time, the helium burning will have used up most of the available helium and gradually die out. This will make the upper layers contract again, and thereby heat until hydrogen is again burning in a shell and leaving new helium in the new region it now burns its way through. In this way the two shells – the upper hydrogen burning shell and the inner helium burning shell – will alternate in delivering the energy to the AGB star luminosity during this, the star's double shell phase or TP-AGB phase. Fig. 3.4 illustrates the mechanism.

The upper (right) panel of Fig. 3.4 starts with the "power-on" phase where the helium shell ignites semi-explosively, increasing the energy output toward $10^8 L_\odot$. The strong energy release results in the development of a convective inter-shell, in order for the energy to be transported fast enough upward, and therefore the burning products from the helium burning shell is being moved outward. This first phase is very short, typically just 200 years, and is soon followed by the "power down" phase where the helium burning fall down to a more steady level, and the convective movement in the inter-shell region therefore dies out. In response to the structural changes in the shell and inter-shell regions, the outer convective envelope now starts penetrating downward in what is called *the third dredge-up* phase. Remark that while intermediate-mass stars have a first, second, and third dredge-up, low-mass stars have only a first and a third dredge-up phase. During the third dredge up, the outer convective envelope will develop passed the previous hydrogen burning shell and all the way into the region where the convective zone above the helium burning was. Hereby will not only products from the hydrogen burning be mixed to the surface (as in the second dredge up episode), but even material from the deep helium burning zone will be mixed into the surface layers and spectrum forming regions of the star. After the helium burning has almost stopped completely, the hydrogen burning shell will re-ignite, and slowly burn its way a new bit further out through the star, during a 10^4 to 10^5 years long stable hydrogen-burning period called the "power-off" period, referring to the "off" phase of the helium burning.

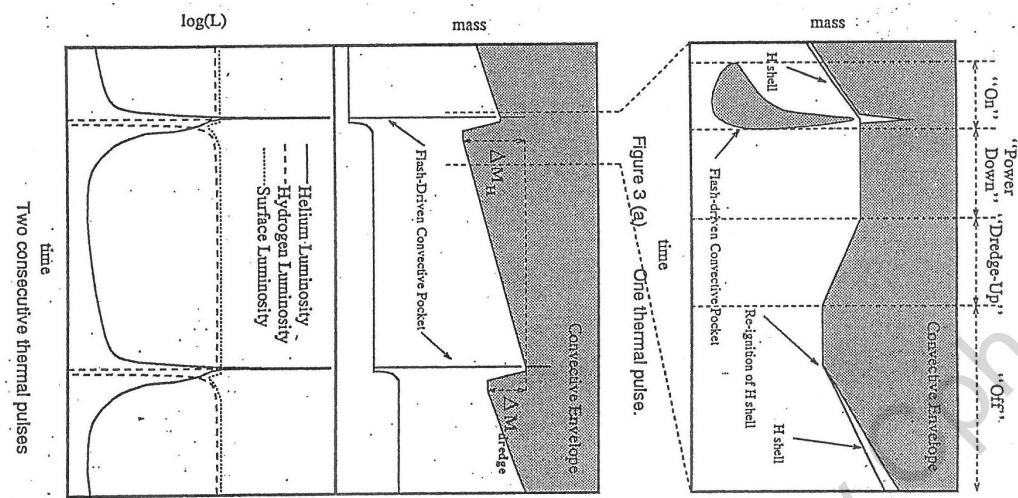


Figure 3.4. A schematic presentation of the alternation between the hydrogen and helium shell burning during the TP-AGB phase of stellar evolution.

The lower (left) panel of Fig. 3.4 illustrates the longer timescale development from one shell flash to the next. One sees how the complete double-shell and inter-shell patterns slowly moves outward through the star. Also shown are the important quantities ΔM_H and ΔM_{dredge} . ΔM_H is the amount of mass that is traveled by the hydrogen burning shell from the time of one helium shell flash to the next. ΔM_{dredge} is the mass coordinate that the convective envelope is moving down through during the third dredge up episode. $\Delta M_{dredge}/\Delta M_H$ is therefore the fraction of newly (hydrogen and helium) processed stellar mass that can be dredged up during a given third dredge up cycle. Since the next helium flash will occur at the bottom of the region the hydrogen shell has moved through, the material that was not dredged up in one cycle, will be part of the material that goes into the explosive helium burning when the next cycle starts with a new power on phase. If the helium burning was nothing but triple alpha burning (Eq. 1.7), then of course this tricky overlap was irrelevant for the final product; in the end all helium would be converted to carbon and the dredge-up product would be pure ^{12}C anyway. However, because of the explosive character of the "power-on" episode, this is the only other place in nature (beside the 4 seconds of supernova explosion per century described earlier) where there is energy enough available to create elements heavier than iron. We will therefore expect conversion of iron to heavier elements together with the carbon production, if the numerical models described here has a reality into them. We will see below that not only have observations shown that this is the case, but quantitative analysis of the spectra of stars that have undergone the third dredge-up episode gives us precise information about how many flashes must have occurred and what temperature and densities must have been in the helium shell flash region.

Since the main burning product of helium is carbon, we will see the star changing from being oxygen-rich (as our own Sun) to being carbon rich, along with successive repetitions of the third dredge-up episode bringing up more and more carbon to the surface. Because of the large dissociation energy of the CO molecule (larger than any other abundant molecules in stellar atmospheres), a stellar atmosphere with more carbon than oxygen will appear very different from one with more oxygen than carbon. If $\text{C}/\text{O} < 1$, there will be free oxygen available after all carbon has been locked up into CO, and the spectrum (apart from CO) will be dominated by molecules such as OH, H_2O , TiO, and SiO. If on the other hand $\text{C}/\text{O} > 1$, there will be free carbon available after all oxygen has been locked up into CO, and the spectrum (apart from CO) will be dominated by molecules such as C_2 , CH, CN, C_3 , C_2H_2 , and HCN. The difference between these two types of spectra is actually so large that one can see the difference with the naked eye. The much stronger absorption of blue light by the carbon-rich molecules than the oxygen-rich molecules, makes the carbon-rich stars much redder than any other type of star (unfortunately there are no bright carbon stars in our night-sky, so one will need a small telescope to see it). In a spectrum, the difference is striking.

3.2 The *s-process* elements formation site.

The strongest reason why we believe that the *s-process* elements are created in (the chemically peculiar) red giants, is that we see the *s-process* elements strongly enhanced in the spectra of these stars, in particular in the cool *N-type* carbon stars. It is more than half a century ago now that it was first realized that red giant stars is a production site for heavy elements – long before any numerical model was able to include such details in the stellar evolution computations. In 1950 S.Merill published a now famous paper where he demonstrated that a group of red giant stars showed lines from the heavy element technetium in their spectra. A peculiar thing about Tc is that it has only radioactive isotopes – no stable isotopes. The fact that the spectra showed technetium, therefore clearly showed that these elements had been mixed into the spectrum forming upper region of the star no longer than a few half-lives after they had been formed in a nucleosynthesis in the stellar interior. It was the first time ever that anybody had seen direct traces of the nuclear burning processes from the interior of any star. Technetium is an *s-process* element, and since stars that are enriched in *s-process* elements are always also enriched in carbon, we are now quite sure that it is the same process that creates the carbon (the triple α process described above) which as a bi-product under certain conditions also creates the *s-process* elements.

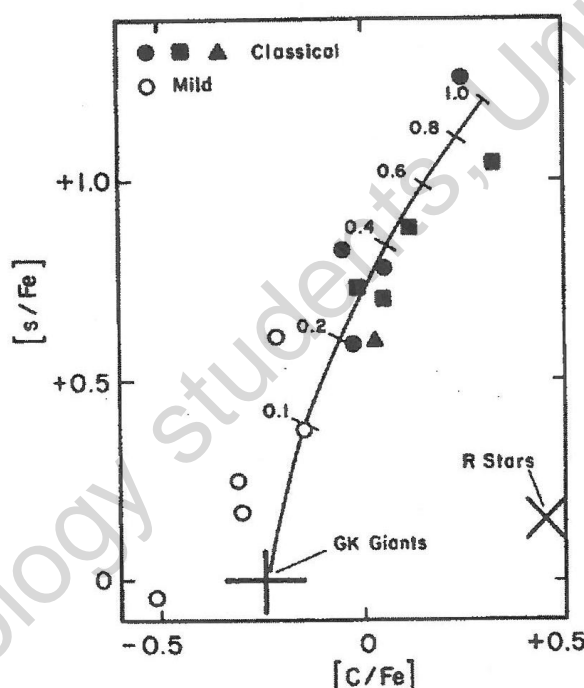


Figure 3.5. The abundance of *s-process* elements versus the abundance of carbon. All abundances are normalized to the abundance of iron, and these abundance ratios in the stars (e.g. $(s/\text{Fe})_*$) are then expressed relative to the corresponding solar ratio (e.g. $(s/\text{Fe})_{\odot}$): $[s/\text{Fe}] = \log[(s/\text{Fe})_* / (s/\text{Fe})_{\odot}]$. The meaning of the other symbols and lines are explained in the text.

Fig. 3.5 shows the abundance of the *s-process* elements as function of the carbon abundance in some red giants. The dots are observations while the solid line represent the correspondence one would get by adding the fraction indicated along the line of an *N-type* carbon star atmosphere onto a normal (i.e., almost solar composition) *GK-type* giant. Beside showing the correspondence between carbon and *s-process* elements, this figure therefore also indicate that these stars are formed from normal stars by pollution with mass from a carbon star. The figure also shows that the *R-type* stars (which are warmer carbon rich stars than the *N-type* carbon stars) are not enriched in *s-process* elements but only enriched in carbon, which tells us that the correspondence is not so simple that *s-process* elements are always created when carbon is produced.

In order to produce *s-process* elements, it is necessary that free neutrons are present. Since free neutrons

are unstable and decay with a half-life of ~ 10 minutes, they must be produced together with the carbon production, but obviously, Eq. 1.7 does not give neutrons by itself, so something else must be associated with the carbon production, which is not directly associated with Eq. 1.7.

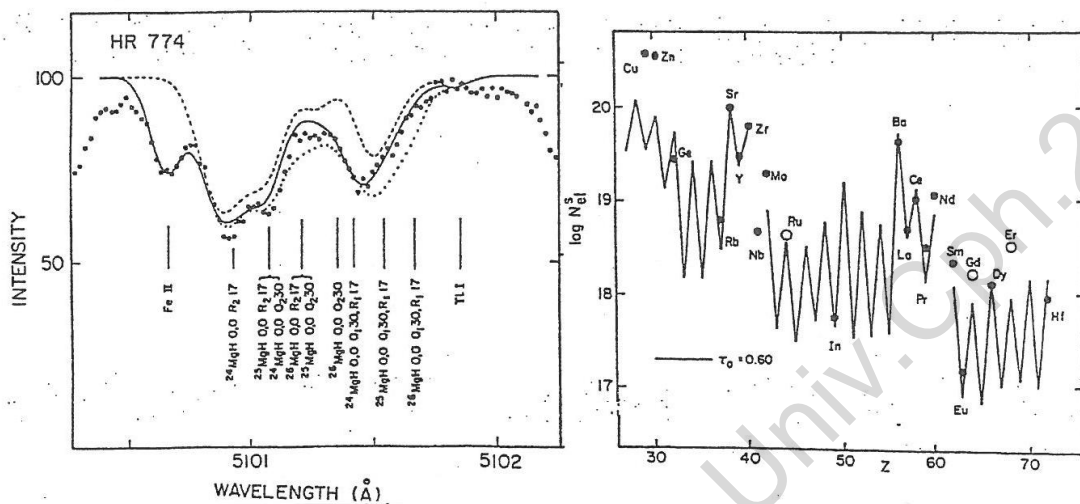
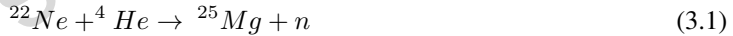


Figure 3.6. Left panel: The observed spectrum of the Ba-type red giant HR 774 (big dots) compared to 3 synthetic spectra computed under the assumptions of including spectral lines from (1) only C₂ (dashed line), (2) C₂+MgH with the terrestrial mixture $^{24}\text{Mg}:\text{Mg}^{25}:\text{Mg}^{26} = 79:10:11$ (solid line), and (3) C₂+MgH with equal abundances of the Mg isotopes (dotted line). Right panel: The observed abundances in HR 774 compared to the predicted abundances, $\log N_{el}^s$, of elements from Cu to Hf based on a distribution function, $\exp(-\tau/\tau_0)$ with $\tau_0 = 0.6$. From Lambert 1985.

Fig. 3.6 (left panel) shows the observed spectrum (dots) of a barium-rich red giant compared with observed spectra in a region where C₂ and MgH dominates the spectrum. It was for a long time believed that the reaction



would be responsible for producing the neutrons that should carry the *s*-process in the region where also the carbon is produced in cool carbon stars. If this reaction was the responsible neutron source, then numerical calculations showed that one should expect a resulting ratio between the Mg isotopes $^{24}\text{Mg}:\text{Mg}^{25}:\text{Mg}^{26}$ of approximately 1:1:1. The spectrum one would then expect to observe is shown in Fig. 3.6 as the dotted line. It is seen that in particular for the feature around 5101.5 Å where the less abundant isotopes 25 and 26 were expected to play a role, the observed spectrum is in clear disagreement with this hypothesis of the neutron source. We now believe that the reaction in Eq. 3.1 is active only in the relatively rare highest mass carbon stars and/or only for a relatively short time in lower mass stars, while the reaction



is active in the bulk of the carbon stars and give rise to formation of the bulk of the *s*-process elements we see in nature.

Sometimes it is convenient to list the whole chain of reactions that take place rather than just a start and end product of the reaction or a central single part of the reaction as is done in Eq. 3.1 and 3.2. In order to include the whole set of reactions, the symbolism with arrows is not convenient, and it is then more common to write the reactions in the form of parentheses, such that for example Eq. 3.2 would be written as $^{13}\text{C}(\alpha, n)^{16}\text{O}$, and the whole reaction chain starting with 3 alpha particles (helium nuclei) ending with oxygen could be written in a compact and informative way as



The calculated abundances of the *s-process* elements depends of course on the physical conditions in the medium where the reaction is supposed to take place, primarily the temperature and the number of free neutrons present. The result of course also depends on the number of relevant nuclei present, but it turns out that in reality the situation is more simple than one could have feared a priori. The lightest nuclei have rather small cross section for the reaction with neutrons, and the heaviest nuclei have very small abundances. Therefore the iron group elements are the dominant seeds for the neutron radiation in the build up of heavier elements. In practice it turns out that it is a good approximation to assume that all reactions start with ^{56}Fe .

The neutron exposure, τ , (or irradiation or fluence) is defined as

$$\tau \equiv \int n_n < v > dt \quad (3.4)$$

where n_n is the number density of neutrons and $< v >$ is the average relative velocity of the neutron and the target nucleus, and the integral is over the time of the exposure. However, calculations based on a single exposure of the observed material to neutrons, fail to reproduce the observed spectra. Instead it was early realized that many exposures of the material with a probability distribution of the exposure times resulting in a distribution of exposures given by

$$p(\tau)d\tau = e^{-\tau/\tau_0}d\tau/\tau_0 \quad (3.5)$$

gave a much better fit to the observations. In the right panel of Fig. 3.6 is shown the predicted abundances of the elements from Cu to Hf (solid line) compared to the observed abundances in the star HR 774, based on a neutron exposure distribution function as in Eq. 3.5 with $\tau_0 = 0.3$. This value of τ_0 also gives a good agreement between predicted yields from carbon stars and the observed relative abundances of the solar system *s-process* elements.

Although almost all of the *s-process* isotopes show evidence for reactions where the time-scale for a neutron capture was much longer than the β decay time scale, there are a few places in the β stability valley where these time-scales seem to be of the same order of magnitude, for example around ^{85}Kr and ^{86}Rb . At such places one sees evidence of a branching in the route of the nuclei, and the relative ratios of the nuclei is then a measure of the temperature, densities, and exposure time-scales at the place of the *s-process* formation. From comparing the relative abundances of isotopes around such branchings, it is inferred that the *s-process* takes place at $\approx 10^8$ K at a density of $\approx 10^8$ neutrons per cm^3 .

We saw above, during the discussion of the numerical results from the third dredge-up episode, that at any given dredge-up, a fraction

$$r = \Delta M_{\text{dredge}} / \Delta M_H \quad (3.6)$$

of the material that is part of the convective region where the neutrons are produced, was also part of the previous helium shell flash convective region, while a fraction $1 - r$ is exposed to neutrons for the first time. If the exposure $\Delta\tau$ of neutrons is the same in each shell flash and the ratio r is also the same, then the fraction $1 - r$ has received only a neutron exposure $\Delta\tau$, a fraction r has received a total neutron exposure of $2\Delta\tau$ or more, a fraction r^2 has received an exposure $3\Delta\tau$ or more, etc. This finally leads to an exponential distribution of the form of Eq. 3.5 of the probability for having received various neutron exposures. All this is consistent with, and therefore pointing at, the carbon stars as the origin of the *s-process* elements in the universe.

While it seems correct to state that the $^{22}\text{Ne}(\alpha, n)^{25}\text{Mg}$ is not the dominant neutron source, and that the best other guess is $^{13}\text{C}(\alpha, n)^{16}\text{O}$, then it is still only poorly understood how there can be enough ^{13}C available to produce sufficient neutrons during the shell flashes, for production of the observed abundance of *s-process*-elements. Some modelers have decided just to assume that a sufficient amount of ^{13}C is somehow introduced into the inter-shell region, and continues the calculations from thereon to predict e.g. the relative amount of various *s-process*-elements, given different physical conditions. One possible mechanism that could be responsible for the production of the necessary amount of ^{13}C , could be the injection of protons downward from the bottom of the convective envelope during the beginning of the "power-off" or interpulse period where the convective envelope reaches a maximum inward penetration. Some numerical codes actually do predict such an inward mixing, by invoking so-called "semiconvection" or overshooting in the scheme, which means that convection stretches beyond the classical convection edges.

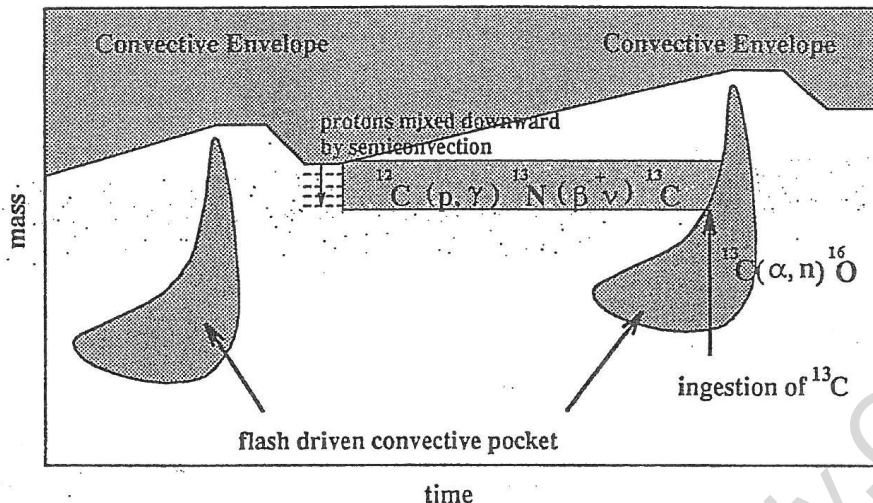


Figure 3.7. A schematic presentation of how semiconvection can be envisioned to ingest protons into the inter-shell region, creating ^{13}C , and how this ^{13}C can then become the source for the neutron production during the next helium shell burning episode, which would then in turn lead to formation of s-process elements.

Figure 3.7 shows how semiconvection would result in a release of neutrons. The inter-shell region between the hydrogen burning shell and the helium burning shell, typically contain 75% ^4He and 25% ^{12}C . Protons mixed down into the hot intershell region would immediately react with the present ^{12}C and form ^{13}C (following reaction Eq. 3.3). The ^{13}C would then capture one of the many ^4He nuclei, which would result in the production of a ^{16}O nuclei and a neutron. If the $^{13}\text{C}(\alpha, n)^{16}\text{O}$ reaction takes place under the conditions of the inter-flash period, it is predicted to result in a low neutron density of $\approx 10^7$ neutrons per cm^3 , while reactions during the helium shell flash is predicted to result in a higher neutron density of $\approx 10^9$ neutrons per cm^3 . Both are close to the range inferred from observations, as described above.

If ingestion of protons from the convective envelope is really the explanation for the production of ^{13}C , then it has interesting consequences for the probabilities for forming Earth-like planets. The downward mixed protons will mainly react with carbon, because there is most of this element (next after ^4He which the proton cannot react with due to the lack of atoms with mass number 5). However the proton will also react with trace elements of many other nuclei, among them ^{25}Mg which will be transformed to ^{26}Al . The latter is radioactive with a half life of 700,000 years, and if it was mixed to the stellar surface and brought into interstellar space at the right amount and at the right time, it could have been included into the protosolar nebula that became our planetary system. The planets are known to have contained a relatively large amount of ^{26}Al at the time of their formation, and it might have played a very important role for melting the protoplanets. If the protoplanets had not melted, no iron core had formed in our Earth, there had been no magnetic field, and maybe no oceans. For sure the physical surroundings on our globe had looked very different if ^{26}Al had not been present during the solar system formation. But it has to have been ingested into the solar nebula right before the planetary formation, otherwise it would have decayed (to the non-radioactive ^{26}Mg) before the planet collected solid material for their formation. It is not known where this radioactive material came from. It might have come from a nearby supernova explosion and it might have come from the inter-shell region of one or more nearby red giant stars. Both possibilities have their theoretical advantages and problems. However, if the process that ingested the radioactive material into our solar system is rare, we might find other solar systems with Earth mass planets in Earth-like orbits around Sun-like stars, but with very different conditions on the surface of these planets anyway, compared to those that allowed life to develop on our planet. We will return to the discussion of ^{26}Al in connection with the discussion of the formation of the solar system.

To summarize, we have now seen that the *s*-process elements can be enhanced in carbon type red giants,

we argued that the temperatures and neutron densities where the observed *s-process* elements formed must have been of the order of 10^8 K and 10^8 neutrons per cm^{-3} , and we have also concluded from the observations that the $^{13}\text{C}(\alpha, n)^{16}\text{O}$ must be responsible for the neutrons, and we have got evidence for the complicated convective movement described by the theory, from the seeming exponential exposure of the material to neutron fluxes. All this, however, only explains why the red giant spectra looks the way they do. In order to have shown that these stars actually are responsibly for half of the elements in our surroundings, including the biological carbon and the nitrogen in our body, and 2/3 of the elements heavier than iron, then we still need to analyze whether these newly produced elements actually can come out of the star and into the interstellar space, such that new stars and planet like our own can be made out of this material. We have already seen that almost all white dwarfs have a mass of precisely $0.55 M_{\odot}$, independent of which mass they started their life with. We are therefore pretty confident that low-mass stars somehow must be able to return most of their material into the interstellar space, even though they never explode, such as high-mass stars do when they become supernovae. The explanation about how this return of mass from low-mass star are thought to take place, is closely related to the formation of dust in the AGB stellar envelope, which is the subject of the next section.

3.3 Dust formation – the driving force of mass loss during AGB

The bulk of the solid material that makes up the planets in our solar system, is condensed out of the gas-phase in the disk that surrounded the protosun during the very beginning of the solar system formation. The timescale for the planet formation was very long compared to the timescale for condensation of various monomers that must have been present in the gas-phase of the protosolar nebula. We can therefore assume that the solid material condensed out of the nebula in thermodynamical equilibrium with the gas. This is a strongly simplifying condition, that will allow us to write a set of relatively simple equations for the solid material that formed the different planets of different composition at different distances from the Sun; predictions that turn out to be in quite good agreement with the overall appearance of our present-day solar system. We will return to these equations and their implications for the formation of planets in the chapter about the solar system formation. However, there are very few places in the Universe where the dust formation is this simple. At almost all other locations, the timescales for the formation of the dust are comparable or longer than the dynamical timescales of the object, as is summarized in Tab. 3.1.

Object	Temperature [K]	$\log n_{<\text{H}>}$ [cm^{-3}]	$\log t_{\text{typ}}$ [s]	$\log t_{\text{cond}}$ [s]		
				SiO	Fe	C
<i>interstellar medium</i>						
H II regions	10000	2 – 3	≈ 12	∞	∞	∞
Intercloud medium	10000	≈ -1	?	∞	∞	∞
Diffuse clouds	100	≈ 2	?	> 18	> 18	> 18
Dark clouds	10 – 20	≈ 4	?	> 18	> 18	> 18
Molecular clouds	50	≈ 6	≈ 15	> 18	> 18	> 18
Compact H II-reg.	100 – 1000	3 – 4	≈ 11	≈ 13	≈ 14	13 – 14
<i>explosive ejection of matter</i>						
Novae	from 10000 down	$\leq 8 - 10$	6 – 7	$\approx 6 - 8$	7 – 8	7 – 8
Supernovae	from 10000 down	7 – 9	7 – 8	$\approx 7 - 9$	8 – 10	8 – 10
<i>massive winds of giant stars</i>						
Cool winds	from 2000 down	7 – 10	≈ 8	$\approx 7 - 9$	≈ 8	≈ 8
Hot winds	from 20000 down	6 – 8	≈ 6	$\approx 8 - 10$	$\approx 9 - 10$	≈ 9

Table 3.1. Timescales and physical conditions in various objects in the universe, and the corresponding timescales for the formation of 3 kinds of abundant dust grains under the physical conditions of these objects.

In those cases the computation of the dust formation is much more complicated. We will not go in to the details here, but only qualitatively sketch the solution in Fig. 3.8. Outward through the stellar atmosphere, the temperature decreases (upper panel). Typical condensation temperatures are around 1300 K (shown as a dash-dot vertical line through the figure). In principle an increasing fraction of the gas will condense when the temperature gets even lower, but further out in the atmosphere also the density will decrease (second panel), so the probability for collision between the monomers (or grain and monomer) will decrease. The competition between the effects of the decreasing temperature and the decreasing density, will result in an effective lower temperature for formation of new dust grains (nucleation) at around 700 K (the second vertical dashed-dot line). The nucleation of dust is only poorly understood, but basically the theory says that it is energetically beneficial to split clusters into single monomers (an atom or a molecule, f.ex. Fe, C, or SiO) if the cluster is smaller than the critical cluster size N^* . Only if the cluster gets larger than the critical cluster size, will it be energetically beneficial to add further monomers to the cluster. The regime where clusters consist of more than N^* monomers is therefore called the growth regime. While the gas and dust moves outward through the upper atmosphere, the dust grains will grow until there are no more monomers left in the gas or (more usual) until the gas-density has become too small for the collision probability to be large enough for further dust growth.

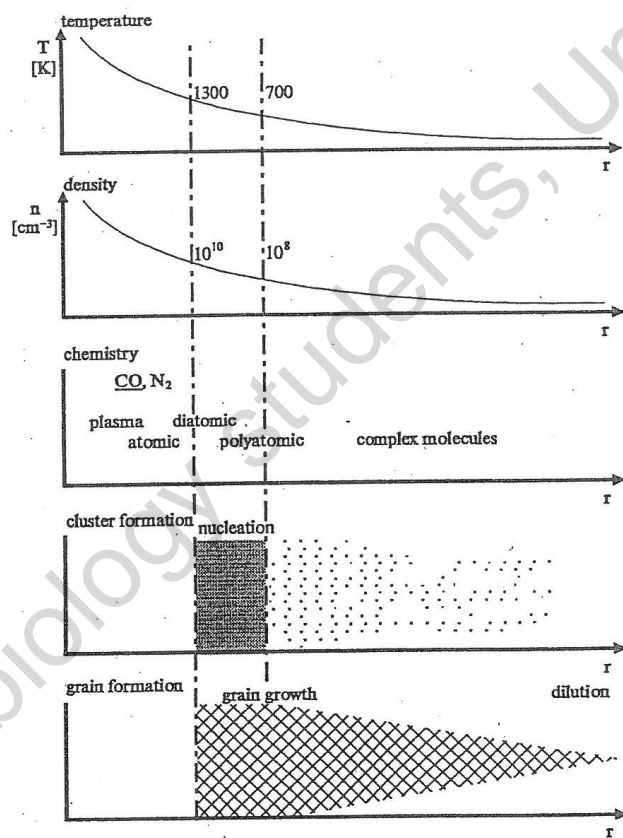


Figure 3.8. Schematic illustration of the dust nucleation and dust growth regime in a stellar wind from a TP-AGB star. The nucleation sets quite abruptly in when the temperature gets below the dust condensation temperature (here 1300 K), and nucleation, and in particular growth, of dust continues until either the dust-monomers are exhausted from the gas or the density has become so low that the collision probability with the monomer effectively has become zero.

Table 3.1 shows a compilation of timescales for various objects, and the corresponding timescales for dust formation under the physical conditions (temperature, pressure, etc) in these objects. It is seen that only in the wind from cool stars, in nova outflows, and in the gas from supernova explosions are the timescales such that we can expect the formation of solid material (dust). Whenever a gas condense into solid dust grains, the opacity of the material increases enormously. We know this process from daily life, where the transparency

of the atmosphere increases markedly when trace amounts of gaseous water condense into droplets (clouds). In stellar (f.ex. cool stars like red giants) environments the radiation is produced inside the star, and have to eventually shine into space in order to keep in balance with the energy production. The force this radiation acts with on the gas is usually small compared to the force expelled by the thermal movement of the gas, and at best it contribute to expand the gas a bit, until a static balance is reached where the gas is diluted enough that the radiation can escape the star. When the gas condense into dust grains in the outer part of the stellar atmosphere, the situation is, however, often quite different. In this situation, the ability of the material to absorb radiation (the absorption coefficient), may increase with several orders of magnitude. The material now blocks enough light that the radiative force per gram of the material due to its increased ability to block the light, may often exceed the gravitational force by the star. The dust grains are then accelerated out of the star's gravitational field (i.e., into interstellar space). Usually the thermal collisions between the dust grains and the gas, will pull the gas outward with the dust.

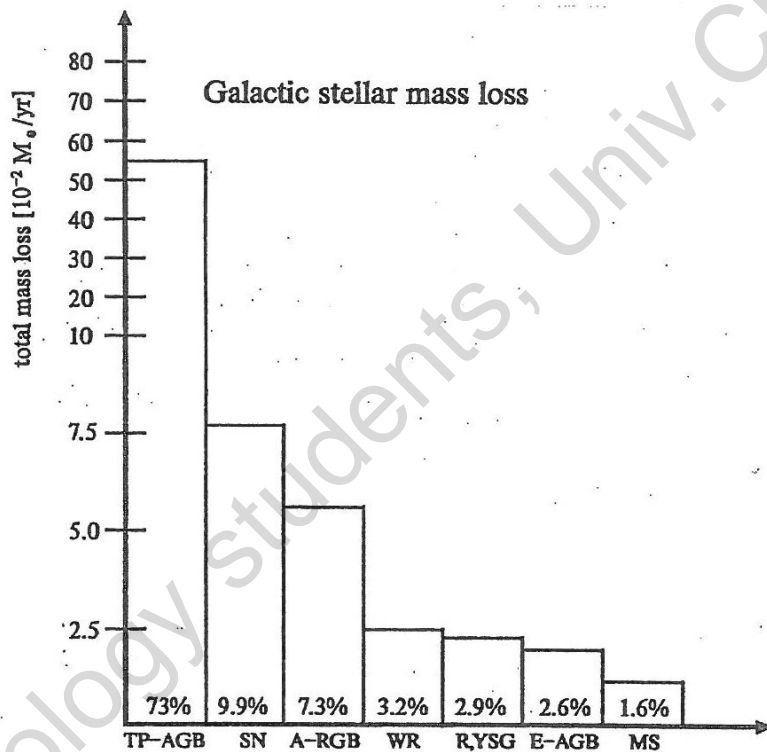


Figure 3.9. The estimated total amount of mass loss (in $0.01M_{\odot}$ /year) from all existing stars in our Galaxy. Along the histogram is also given the relative distribution to the mass loss of all the listed types. It is seen that the TP-AGB stars are estimated to be responsible for most (73%) of the material that is returned to interstellar space, while super nova is on a second place with estimated 9.9% of the total Galactic stellar mass loss.

In this way we have created a dust driven stellar wind. Although the detailed mechanism of the dust driven winds are not understood, it is believed that this mechanism is the physics that make the stars loose most of their mass into interstellar space. In particular carbon rich dust has a high absorption coefficient (we know this from daily life too, from the black colour of f.ex. active coal powder). It may therefore not be a coincidence that the mass coordinate of the helium shell in red giants at the onset of the TP-AGB phase described above, is approximately the same as the average white dwarf mass shown in Fig. 1.10. When carbon is mixed up to the surface at the onset of (or shortly after) the first explosive helium shell burning, then free carbon will occur after the CO formation (as described above) instead of free oxygen. At the low temperatures of the outer atmosphere of AGB stars, a large fraction of this carbon will form carbon rich dust grains (graphite, amorphous carbon powder, diamond dust, SiC grains, etc). As a result, the absorption

coefficient of the material will suddenly increase tremendously. At the large size of red giant (AGB) stars, the stellar gravity at the top of the atmosphere is quite small (typically 3 to 4 orders of magnitude smaller than on the Earth). The radiative acceleration on the material may therefore suddenly exceed the gravitational acceleration, and the material will move outward. Since new carbon keeps coming up from the interior of the star with each new dredge up episode, the whole envelope may soon blow into interstellar space in the form of a dust driven wind.

Although carbon-rich AGB stars are relatively rare among the total Galactic stellar population, most of the material returned into interstellar space may well come from these stars. Figure 3.9 is a compilation by E.Sedlmayr (1994) from various available sources, that show the relative contribution of different sources to the return of stellar material into interstellar space. His estimate is that 73% of the Galactic stellar mass loss comes from TP-AGB stars. Qualitatively this picture is in agreement with the simple estimates we made in a previous chapter about the ratio between the mass loss from high-mass stars and low-mass stars, and it is also in qualitative agreement with the considerations above, about the mixing of material from the helium shell and the white dwarf mass function. Also the fact that 2/3 of the elements in nature that are heavier than iron are produced in TP-AGB stars, indicate that the mass loss from these stars must be substantial. Finally the fact that the isotopic $^{12}\text{C}/^{13}\text{C}$ ratio in carbon stars near the end of their lives is the same as the isotopic ratio of carbon on the Earth (and not e.g. the very different CNO-equilibrium value from Tab. 1.2), brings an additional clue that the carbon in our body probably was produced during the explosive helium shell flash burning in TP-AGB stars. Some of the most abundant extrasolar dust grains (diamond dust) that we find in primitive meteorites do also have this $^{12}\text{C}/^{13}\text{C}$ ratio, in spite of the ^{12}C and the ^{13}C , as we have seen above, are being made during two completely independent processes in stellar evolution.

For astrobiology students,
Version 2.3, February 9, 2023